A mathematical model and design tool

KOLEKTOR 2.2

reference handbook (3rd draft, 01-2009)

developed by: Ing. Tomas Matuska, Ph.D.,

(theoretical part of the model)

Ing. Vladimir Zmrhal, Ph.D.

(Visual Basic program)

Czech Technical University in Prague, Faculty of Mechanical Engineering, Dept. of Environmental Engineering

Technicka 4, 166 07 Prague 6

Email: tomas.matuska@fs.cvut.cz

Content

1. Introduction

Computer modeling of solar thermal collectors is a principle approach for testing of new construction concepts and improvements in the development and design stage for developers and manufacturers. Virtual prototyping of solar collectors can save the investments into number of prototypes and foreseen the collector performance in advance. Analyses of individual construction parts and details parameters impact on the collector performance is needed to make decision on efficient solar collector concepts for given application, operation and climatic conditions with respect to economic parameters of solar collector construction.

A mathematical model is always a simplification of reality to certain extent. Too complex mathematical models and numerical programs require huge amount of computer time for calculations, too simplified models don't take important influences of detailed collector parameters into account and result in considerable uncertainty in calculation. To find a good compromise between simplicity of the model and required level of accuracy is crucial for development of any design and simulation tool.

Although the theory of flat-plate solar collectors is well established and can be found in basic solar engineering literature [1-3], there is a lack of user-friendly design programs for solar collector performance modeling considering the detailed geometrical, thermal and optical parameters of collector. Number of authors evolved simplified analytical models considering temperature independent solar collector overall heat loss coefficient (linear dependence of efficiency), neglecting the absorber temperature distribution or temperature difference between absorber surface and heat transfer fluid. Such models are not comparable with physical experiments and cannot predict the real performance behavior and evaluate the energy output and efficiency characteristics of solar collectors.

Theoretical model of solar thermal collector has been introduced in TRNSYS Type 73 [4] but with simplified calculation of collector heat loss coefficient *U* insufficient to cover wide range of parameters affecting the collector heat loss. More theoretical model with number of detailed input parameters and calculation of heat transfer coefficients in the individual parts of collector (in air gaps, inside pipes, at outer surfaces) has been evolved as TRNSYS Type 103 [5].

A design program CoDePro [6] for energy performance calculation of solar flat-plate collectors has been developed with the Energy Equation Solver. It allows a very detailed specification of collector geometrical and material parameters (thermal, optical). It covers the basic segment of solar collectors (unglazed, single and double glazed) and evaluates also optical properties of collector in detail, e.g. incident angle modifier. On the other hand, the features of CoDePro program, analogous to TRNSYS Type 103, don't allow energy performance modeling of advanced solar collectors, e.g. collectors integrated into building envelope, evacuated flat-plate collectors, rare gas filled collectors or solar collector with glazing made of transparent insulation structures.

The presented model and design tool KOLEKTOR 2.2 has been developed to overcome the drawbacks of previous models. KOLEKTOR 2.2 is based on detailed calculation of heat transfer from the collector absorber to ambient and from the collector absorber to heat transfer fluid. The advantage of the design tool is its universality to wide-range of solar flat-plate collectors stock from evacuated to

atmospheric, separately or building integrated, covered with different types of glazing (single glazing or transparent insulation structures), etc.

2. Mathematical model

2.1. Outline of the model

The core of the design tool KOLEKTOR 2.2 is a mathematical model of solar flat-plate liquid collector solving one-dimensional heat transfer balances. Detailed geometrical, thermal and optical properties of individual elements of solar collector, climatic and operation conditions are the input parameters of the model. Basic outputs of the model are usable heat gain $\dot{Q}_u$, efficiency η with respect to reference collector area (aperture area A_a) and output heat transfer fluid temperature t_e. The advanced outputs as heat transfer coefficients, temperatures of main surfaces in collector layout and stagnation temperature can be also obtained from the model.

The mathematical model of solar collector consists of external energy balance of absorber (heat transfer from absorber surface to ambient environment) and internal energy balance of absorber (heat transfer from absorber surface into heat transfer fluid). Model solves the energy balance of the solar collector under steady-state conditions according to principle Hottel-Whillier equation for usable thermal power

$$\dot{Q}_u = A_a F_R [\tau\alpha G - U(t_{in} - t_a)] \tag{2.1}$$

Through the external energy balance of absorber the heat transfer by radiation and by natural convection in the air gap between absorber surface and glazing (event. frame), heat conduction through glazing (event. frame) and heat transfer by convection and radiation from exterior glazing (event. frame) surface to ambient is solved. To calculate the heat transfer coefficients properly, temperatures for principal collector levels (surfaces) should be known, but on the other side the temperature distribution in the collector is dependent on the heat transfer coefficients values. Therefore, external energy balance of absorber is solved in an iteration loop starting from first estimate of temperatures for each main surface based on given input temperature t_{in} and ambient temperature t_a. The absorber temperature t_{abs} required in the calculation is estimated in first iteration cycle of external balance from t_{in} by relationship

$$t_{abs} = t_{in} + 10\,\mathrm{K} \tag{2.2}$$

External balance loop yields in overall heat loss coefficient U of the collector.

Internal energy balance of absorber assesses the heat transfer from the absorber surface into heat transfer fluid provided by fin heat conduction, by heat conduction through the bond between absorber and pipes and by forced convection from interior surface of pipe to fluid. Internal energy balance results in determination of collector efficiency factor F' and collector heat removal factor F_R on the basis of input parameters, operational and climatic conditions and results from external balance. Main outputs from internal balance are output fluid temperature t_e, mean heat transfer fluid temperature t_m and particularly the absorber temperature t_{abs}, which governs the calculations in the external energy balance. Internal energy balance proceeds in its own iteration loop with respect to relative dependence between mean fluid temperature t_m and forced convection heat transfer coefficients in absorber pipe register. In the first iteration cycle of internal energy balance, the mean fluid temperature is estimated from t_{in} by relationship

$$t_m = t_{in} + 10\,\mathrm{K} \tag{2.3}$$

As both external and internal energy balances are mutually dependent, superior iteration loop has been introduced to transfer the results from external energy balance to internal (overall collector heat loss coefficient U) and from internal energy balance results to external balance (absorber temperature t_{abs}).

2.2. Geometry of solar flat-plate collector

Considered solar flat-plate collector geometry is shown in *Fig. 2.0*. Aperture height L_a is considered same as riser pipe length. Aperture width H_a divided by number of risers n_r gives absorber fin width W (distance between two risers). Sum of frame thickness d_{fr}, front side gas layer thickness d_p, back side gas layer thickness d_z and glazing thickness d_{gl} gives total depth of collector B.

Reference collector area is aperture area (most important for performance behavior assessment).

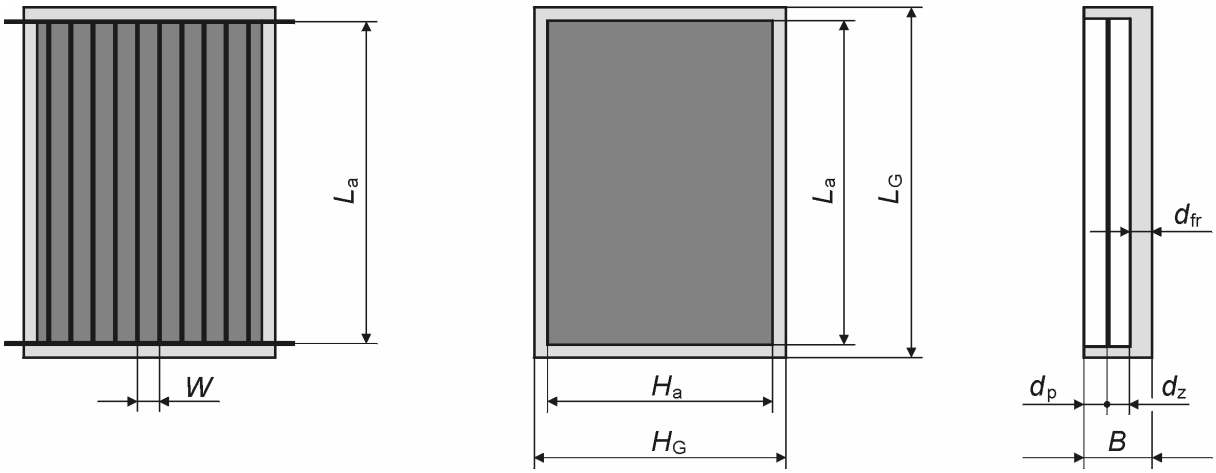

Fig. 2.0 – Solar collector main dimensions and areas

2.3. External energy balance of the absorber

General external energy balance of the absorber can be described by Equation (2.4) given in differential form

$$\frac{\mathrm{d}Q}{\mathrm{d}t} = \dot{Q}_s - \dot{Q}_{l,o} - \dot{Q}_{l,t} - \dot{Q}_u \qquad (2.4)$$

where

dQ/dt	is	change of heat content in collector;
$\dot{Q}_s$		solar irradiation incident on collector area, in W;
$\dot{Q}_{l,o}$		optical loss, in W;
$\dot{Q}_{l,t}$		heat loss, in W;
$\dot{Q}_u$		useful thermal power from collector, in W.

Heat momentum term is influenced by thermal capacity of individual elements of solar collector, irradiation, temperature change and heat transfer liquid flowrate at entrance of the collector. For a number of modelling applications, dynamic model of solar collector is necessary for collector performance calculation at real variable

boundary conditions. The model and design tool KOLEKTOR is developed primary for evaluation of collector performance, comparable with experimental testing under steady state conditions (term dQ/dt = 0). Small heat capacity of flat-plate solar collectors (time constant in order of 10 to 20 minutes) allows also the use of steady state model for longterm balances with time-steps larger than hour.

By expanding the individual terms from Equation (2.4), a detailed balance is obtained in Equation (2.5)

$$\dot{Q}_{\mathrm{u}} = GA_{\mathrm{a}}(\tau\alpha)_{\mathrm{ef}} - U_{\mathrm{p}}A_{\mathrm{G}}(t_{\mathrm{abs}} - t_{\mathrm{a}}) - U_{\mathrm{z}}A_{\mathrm{G}}(t_{\mathrm{abs}} - t_{\mathrm{a}}) - U_{\mathrm{b}}A_{\mathrm{b}}(t_{\mathrm{abs}} - t_{\mathrm{a}}) \qquad (2.5)$$

where

G	is	solar irradiation, in W/m^2;
t_{abs}		absorber temperature, in ℃;
t_{a}		ambient temperature, in ℃
τ		solar radiation transmittance of collector cover glazing;
α		solar radiation absorptance of collector absorber;
U_{p}		heat loss coeffcient for front side of the collector, in W/m^{2}K;
U_{z}		heat loss coeffcient for back side of the collector, in W/m^{2}K;
U_{b}		heat loss coeffcient for edge side of the collector, in W/m^{2}K;
A_{a}		collector aperture area, in m^2;
A_{b}		collector back side area, in m^2;
A_{G}		collector gross area, in m^2.

2.3.1. Heat transfer in solar collector

Calculation of collector heat loss can be performed in several ways. Approximative calculation procedure, often used in practice, for direct overall collector heat loss calculation, is based on empirical complex equation, first developed by Hottel and Woertz [7], modified and reworked by number of authors [8 - 11]. The calculation equation is usable within the certain range of values of design parameters. Simplifications results in uncertainty, which can achieve quite high value (up to 30 %) in specific configurations of parameters. Concerning to general suitability of given equation, the applicability is possible to multiple glazing, atmospheric nature of collector, not for advanced evacuated collectors (transparent insulation).

The calculation of overall collector heat loss by the model is completely different and more detailed. The model solves the heat transfer coefficients from absorber to ambient through front side (gas layer and cover), through back and edge side (gas layer and insulation frame)[1]. Solar collector is defined by means of main levels: glazing exterior surface (p1), glazing interior surface (p2), absorber (abs), frame interior surface (z2) and frame exterior surface (z1). Ambient environment is labeled with (a). These levels are schematically outlined in Fig. 2.1.

[1] In KOLEKTOR 2.2, for the edge side is considered the identical construction as for back side. Edge side will be treated and calculated separately in next software version.

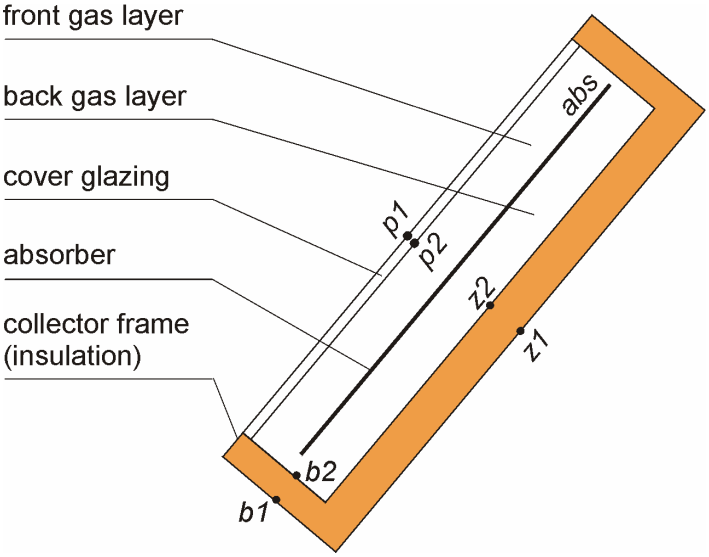

Fig. 2.1 – Main temperature levels (surfaces) in solar collector model.

The simplified scheme of external heat transfer balance model for the solar collector is shown in *Fig. 2.2*. The heat transfer in collector can be described by:

- radiation between absorber and interior surface of cover glazing, resp. interior surface of collector frame (back and edge side);
- natural convection between absorber and interior surface of cover glazing, resp. interior surface of collector frame
- heat conduction through cover glazing and collector frame (insulation)
- radiation between exterior surface of cover glazing and sky dome, resp. exterior surface of collector frame and adjacent surfaces
- natural and forced convection at exterior surface of cover glazing, resp. exterior surface of collector frame

The collector element, the calculated heat transfer coefficient is appropriate to, is defined by pair of indices designating the boundary surfaces (main levels of collector), e.g. gas layer (air gap) between absorber and interior surface of glazing is designated by index *p2-abs.* The principle regimes of heat transfer are designated as: *v* – conduction; *p* – convection; *s* – radiation.

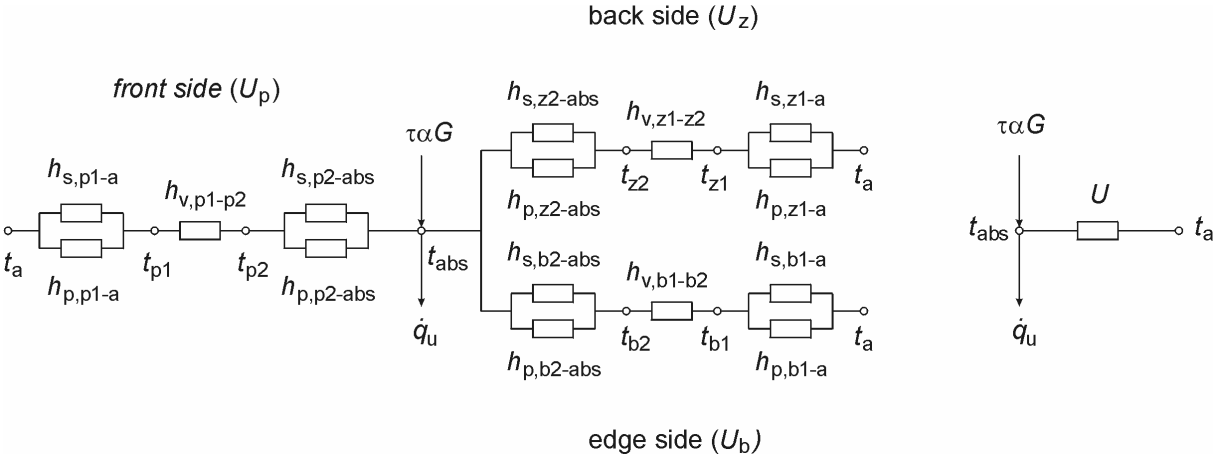

Fig. 2.2 – Schematic detailed layout of external energy balance of absorber and simplified scheme

A literature review to find appropriate theoretical and empirical relationships for heat transfer coefficients calculation has been done by Matuska [12]. For certain heat transfer problems, a number of equations exist from different sources. Several heat transfer models have been integrated in the model and design tool KOLEKTOR to allow the user to choose.

2.3.2. Radiation between glazing and sky ($h_{s,p1-a}$)

To describe the heat exchange between glazing exterior surface and sky, the sky area is considered as a black body of equivalent temperature t_o. Equivalent sky temperature t_o is introduced due to fact that sky temperature is not uniform and constant and atmosphere radiates only in certain wavelengths ranges in reality. At given wavelengths, the atmosphere is transparent (8 to 14 μm), for most others the atmosphere considerably absorbs especially in infrared range. Sky temperature T_o is defined based on absolute ambient temperature T_a [K] as given in Equation (2.6)

$$T_o^4 = \varepsilon_o T_a^4 \tag{2.6}$$

where

ε_o is sky emittance.

Radiation heat exchange between exterior surface of glazing and sky is given by Equation (2.7)

$$q_{p1-o} = \varepsilon_{p1}\sigma(T_{p1}^4 - T_o^4) \tag{2.7}$$

To integrate the Equation (2.7) into collector model the radiant heat flow is divided by temperature difference between exterior surface of cover glazing and ambient environment ($t_{p1} - t_a$)

$$h_{s,p1-a} = \varepsilon_{p1}\sigma\frac{T_{p1}^4 - T_o^4}{T_{p1} - T_a} \tag{2.8}$$

where

ε_{p1} is emittance of exterior surface of cover glazing;

σ Stefan-Boltzmann constant, $\sigma = 5.67\times10^{-8}$ W/m^{2}K^4;

T_{p1} absolute temperature of exterior surface of cover glazing, in K;

T_a absolute ambient temperature, in K.

In literature, a number of correlations for equivalent sky temperature t_o calculation can be found, each obtained for certain boundary conditions, e.g. only for night time (radiant cooling applications), for clear sky conditions, etc. The principle equations express the sky temperature with respect to ambient temperature t_a (dry bulb temperature) [13, 14], to dew point temperature t_{dp} [15, 16], resp. to water vapor pressure p_d [17, 18] or to sky clearness index K_o [18]. Selected equations are given in *Tab. 1*.

Author	**Equation**	
EN 6946 [13]	$T_o = T_a$	cloudy sky
Swinbank [14]	$T_o = 0.0552 (T_a)^{1.5}$	clear sky
Bliss [15]	$T_o = T_a (0.8004 + 0.00396\ T_{dp})^{1/4}$	
Berdahl, Martin [16]	$T_o = T_a (0.711 + 0.0056\, T_{dp} + 0.000073\, T_{dp}^2)^{1/4}$	clear sky
Brunt [17]	$T_o = (0.564 + 0.059\sqrt{p_d})^{1/4}$ $T_o = (0.527 + 0.065\sqrt{p_d})^{1/4}$	p_d [mbar]
Aubinet [18]	$T_o = 94 + 12.6 \ln(p_d) - 13\, K_o + 0.341 T_a$	

Tab. 1 – Selected equations for equivalent sky temperature T_o calculation

Different correlations are suitable for different problem conditions. If calculated results should be compared to solar collector experimental testing at clear sky conditions, it is recommended to use correlation according to Swinbank [14], resp. Berdahl [16] or Brunt [17] if relative humidity φ_a is measured[2]. For model simulating whole year performance of collector based on climatic and operation conditions, the correlation according to Aubinet [18] incorporating the influence of humidity and sky cloudiness. Climatic databases usually contain information on relative humidity φ_a and sky clearness index K_o can be derived from ratio between global solar horizontal irradiation G to solar irradiation incident at exterior atmosphere surface G_o, as given by Equation (2.9)

$$K_o = \frac{G}{G_o} \tag{2.9}$$

Dew point temperature T_{dp} [K] can be calculated according to Equation (2.10) from Berger [19]

$$T_{dp} = \frac{5179.25}{20.519 - \ln\left(\frac{760\ p_d}{101325}\right)} \tag{2.10}$$

[2] Simple equation for equivalent sky temperature according to [14], relating t_o to ambient temperature t_a has been chosen as a default heat transfer coefficient calculation model for design tool KOLEKTOR.

where

p_d is water vapor pressure given by product of ambient air relative humidity φ_a and saturated water vapor pressure p_d'' at ambient temperature t_a [18], in Pa.

with

$$p_d''(T_a) = 611\exp\left(17.27\frac{(T_a - 273)}{(T_a - 36)}\right) \quad (2.11)$$

Comparison of heat transfer coefficients at individual parts of solar single-glazed collector and its influence to front heat loss through cover glazing has shown that radiation exchange between exterior surface of cover glazing and sky dome doesn't affect significantly overall collector heat loss.

2.3.3. Wind convection from glazing to ambient ($h_{p,p1\text{-}a}$)

Heat transfer by convection from exterior surface of collector cover glazing to ambient environment under realistic conditions (natural and forced wind convection) is quite problematic. A large number of relationships and correlations derived from experiments, more or less reproducing the boundary conditions of solar collector installation, can be found in literature. Although the final value of convection heat transfer coefficient is theoretically influenced by collector dimensions, by its slope and air flow yaw angle, turbulence intensity or ratio of free convection, the most of authors keep the correlation as simple as possible resulting in Equation (2.12) in the form of linear function

$$h_w = a + bw \quad (2.12)$$

where

w is wind velocity, in m/s.

Tab. 2 shows different correlations for calculation the convection heat transfer coefficient h_w from literature. Graph in the *Fig. 2.3* shows results for individual wind convection models for case of solar collector characteristic dimension L = 1.3 m, slope 45° and temperature difference 30 K between e xterior surface of cover glazing and ambient air.

It is apparent that there is no common agreement between the models and the results obtained from different correlations can considerably vary within a large range. It is caused by boundary conditions at which individual models have been derived. Correlations obtained from experiments in wind tunnels with low turbulence levels (Sparrow [26, 27]) will produce lower values for h_w than correlations obtained from outdoor experiments (Test [29, 30], Kumar [33], Sharples [34]).

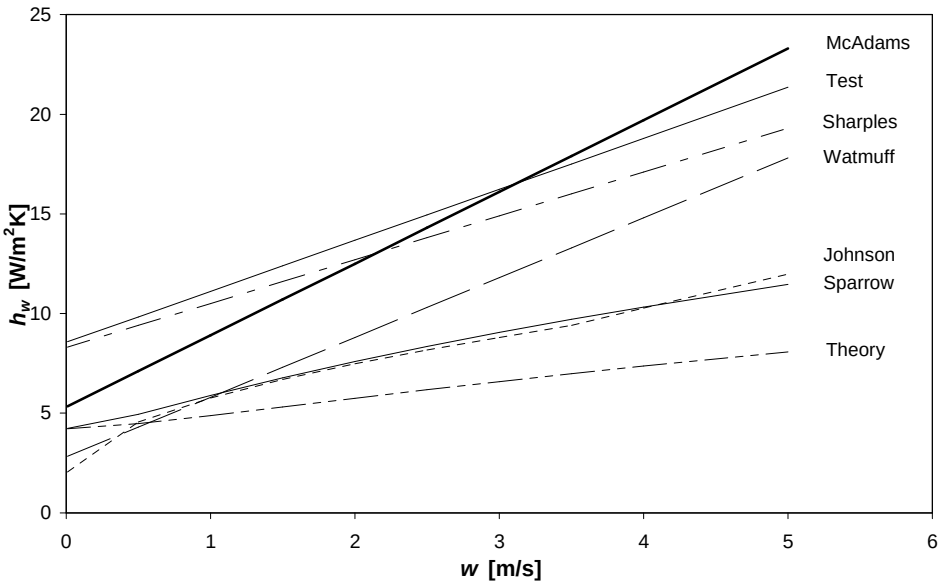

Fig. 2.3 – Comparison of models for h_w calculation

In the solar collector theory, the most used wind convection model is correlation according to McAdams, as given in Equation (2.13):

$$h_{\mathrm{p,p1-a}} = h_{\mathrm{w}} = 5.7 + 3.8w \tag{2.13}$$

which describes the mixed air flow convection and the results lie approximately in the range of values experimentally confirmed by other authors[3].

Author	Equation	Range	Applicability
Forced convection [20]	$\mathrm{Nu}_L = 0.664\mathrm{Re}_L^{1/2}\mathrm{Pr}^{1/3}$		laminar convection
Natural convection Churchill-Chu [20]	$\mathrm{Nu}_L = \left\{0.825 + \frac{0.387\mathrm{Ra}_L^{1/6}}{[1+(0.492/\mathrm{Pr})^{9/16}]^{8/27}}\right\}^2$	for any Ra	natural convection
Mixed convection [20]	$\mathrm{Nu}_L = \sqrt[3]{\mathrm{Nu}_{forced}^3 + \mathrm{Nu}_{natural}^3}$		
McAdams [21, 22]	$h_w = 5.7 + 3.8\,w$ $h_w = 6.47w^{0.78}$	for w < 5 m/s for w > 5 m/s	
Watmuff [23]	$h_w = 2.3 + 3.0\,w$	0 < w < 7 m/s	
Sparrow [24-27]	$h_w = \frac{0.86\rho c_p w}{\mathrm{Pr}^{2/3}\mathrm{Re}^{1/2}}$	2x10^4 < Re < 10^5	
Test [29-30]	$h_w = 8.55 + 2.56\,w$	0 < w < 5 m/s	
Kumar [33]	$h_w = 10.03 + 4.687\,w$	0 < w < 4 m/s	
Sharples [34]	$h_w = 8.3 + 2.2\,w$ $h_w = 6.5 + 3.3\,w$	0.8 < w < 6.5 m/s 0.8 < w < 6.5 m/s	for yaw γ= 0° for yaw γ= 90°

[3] McAdam's correlation has been used as default wind convection model for heat transfer coefficient calculation in the design tool KOLEKTOR.

Johnson, Othieno [35]	$h_w = \frac{\lambda}{L}\left(75 + b_1 \mathrm{Re}^{1/2} \mathrm{Pr}^{1/3}\right)$ $h_w = \frac{\lambda}{L}\left(75 + b_2 \mathrm{Re}^{0.8} \mathrm{Pr}^{0.43}\right)$ slope / Re_{crit} / b_1 / b_2 20° / 1.5×10^{-5} / 1.04 / 0.030 30° / 1.8×10^{-5} / 0.88 / 0.025 40° / 2.5×10^{-5} / 0.80 / 0.020 50° / 3.5×10^{-5} / 0.74 / 0.017 60° / 5.0×10^{-5} / 0.74 / 0.015	$\mathrm{Re} < \mathrm{Re}_{crit}$ $\mathrm{Re} > \mathrm{Re}_{crit}$	

Tab. 2.2 – Selected correlations for wind convection heat transfer coefficient

2.3.4. Conduction through glazing ($h_{v,p1-p2}$)

Thermal conductance of cover glazing is given by

$$h_{\mathrm{v,p1–p2}} = \frac{\lambda_{\mathrm{p1–p2}}}{L_{\mathrm{p1–p2}}} \tag{2.14}$$

where

$\lambda_{\mathrm{p1-p2}}$ is thermal conductivity of cover glazing, in W/mK;

$L_{\mathrm{p1-p2}}$ thickness of cover glazing or transparent cover structure, in m.

In the case of transparent inhomogeneous insulation structures application (e.g. transparent thermal insulations), thermal conductance of the structure should be determined as a function of mean glazing temperature $t_{\mathrm{p1-p2}}$

$$h_{\mathrm{v,p1–p2}} = f\left(t_{\mathrm{p1–p2}}\right) = f\left(\frac{t_{\mathrm{p1}} + t_{\mathrm{p2}}}{2}\right) \tag{2.15}$$

The approach in collector model KOLEKTOR 2.2 is based on the equivalent thermal conductivity of cover glazing structure dependent on the mean temperature in the form of polynomic (2nd order) function in accordance with Equation (2.16)

$$\lambda_{\mathrm{p1–p2}}(t) = \lambda_0 + \lambda_1 t + \lambda_2 t^2 \tag{2.16}$$

Equivalent thermal conductivity function can be easily obtained from thermal conductance function (e.g. from laboratory measurements) and reference thickness of the transparent glazing structure.

2.3.5. Radiation between absorber and cover glazing ($h_{s,abs-p2}$)

Radiation heat transfer between absorber front surface and interior surface of glazing is given by Stefan-Boltzmann law

$$q_{\mathrm{s,abs-p2}} = \sigma \frac{T_{\mathrm{abs}}^4 - T_{\mathrm{p2}}^4}{\frac{1}{\varepsilon_{\mathrm{p2}}} + \frac{1}{\varepsilon_{\mathrm{abs,p}}} - 1} \tag{2.17}$$

where

T_{p2} is glazing interior surface temperature, in K;

T_{abs} absorber surface temperature, in K;

ε_{p2} emittance of glazing interior surface;

$\varepsilon_{abs,p}$ emittance of front absorber surface.

Radiation heat transfer coefficient is given by Equation (2.18)

$$h_{s,abs\text{-}p2} = \frac{q_{s,abs\text{-}p2}}{T_{abs} - T_{p2}} = \sigma \frac{T_{abs}^4 - T_{p2}^4}{\frac{1}{\varepsilon_{p2}} + \frac{1}{\varepsilon_{abs,p}} - 1} \cdot \frac{1}{T_{abs} - T_{p2}} \tag{2.18}$$

which can be rearranged in following way

$$h_{s,abs\text{-}p2} = \frac{\sigma}{\frac{1}{\varepsilon_{p2}} + \frac{1}{\varepsilon_{abs,p}} - 1} \left(T_{abs}^2 + T_{p2}^2\right)\left(T_{abs} + T_{p2}\right) \tag{2.19}$$

to get the equation more suitable for numerical calculations (excluding the division by very small figures at specific boundary conditions).

2.3.6. Natural convection in closed gas layer between absorber and glazing ($h_{p,abs\text{-}p2}$)

Heat transfer by natural convection in the closed gas layer between absorber and glazing is characterized by Nusselt number Nu_L related to characteristic dimension of the layer, the thickness L_g. Geometric parameters of the gas layer and heat flow direction (upward) are outlined in *Fig. 2.4*.

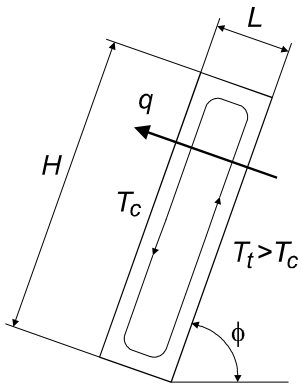

Fig. 2.4 – Natural convection in closed gas layer (heat flow upward)

Relationship between convection heat transfer coefficient h_p for the gas layer and Nu_L is determined by Nusselt number definition

$$Nu_L = \frac{h_p L_g}{\lambda_g} \tag{2.20}$$

Natural convection heat transfer coefficient for closed inclined layer between absorber and cover glazing can be obtained from Equation (2.21)

$$h_{p,abs\text{-}p2} = \frac{Nu_L \lambda_g}{L_{abs\text{-}p2}} \tag{2.21}$$

where

λ_g is thermal conductivity of still gas for mean temperature $t_g = t_{abs\text{-}p2}$ in the gas layer, in W/mK;

$L_{abs\text{-}p2}$ thickness of gas layer between cover glazing and front surface of absorber, in m.

Nusselt number for natural convection is dependent on Rayleigh number Ra_L, i.e. product of Grashof number Gr_L and Prandtl number Pr

$$\mathrm{Ra_L} = \mathrm{Gr_L}\,\mathrm{Pr} \tag{2.22}$$

Prandtl number can be obtained from the properties of used gas at mean temperature of the layer $t_{\mathrm{p2\text{-}abs}}$ as given in Equation (2.23)

$$\mathrm{Pr} = \frac{\nu}{a} = \frac{\nu\,\rho\,c}{\lambda} \tag{2.23}$$

where

ν is kinematic viscosity of gas, in m^2/s;

a thermal diffusivity of gas, in m^2/s;

ρ density of gas, in kg/m^3;

c specific thermal capacity of gas, in J/kgK.

Grashof number $\mathrm{Gr_L}$ is given by Equation (2.24)

$$\mathrm{Gr_L} = \frac{\beta g L^3 \Delta t}{\nu^2} = \frac{1}{T_{\mathrm{abs-p2}}} \cdot \frac{g L_{\mathrm{p2-abs}}^3 (t_{\mathrm{abs}} - t_{\mathrm{p2}})}{\nu^2} \tag{2.24}$$

where

β is volumetric thermal expansion coefficient, (equal to approximately $1/T$, for ideal fluids, where T is absolute temperature), in 1/K;

g gravity acceleration, in m/s^2.

A literature review has been done to find equation for heat transfer coefficient for the case of natural convection in gas enclosure (closed gas layer) with heat flow upward. Suitability of the equation application in area of solar collectors has been limited by following conditions:

- heat flow upward (slope of gas layer ϕ from 0° to 90°), i.e. front gas layer
- high aspect ratio $H/L > 20$
- range of $\mathrm{Ra_L}$ from 10^4 to 2×10^6
- dependence of $\mathrm{Nu_L}$ on the slope of gas layer ϕ, respectively on aspect ratio H/L

Number of published experiments and derived correlations has been found for natural convection heat transfer in sloped enclosure but only several models have been found valid for given boundary conditions. There are especially works of Hollands [36], Buchberg [37] and Randall [38] suggesting the equations based on experimental research with enclosures with different slope and aspect ratio of the gas layer. Schinkel [39] published a simplified correlation for $\mathrm{Nu_L}$ based on own experiments, numeric modeling and use of other previously published data. $\mathrm{Nu_L}$ is in vertical, horizontal or generally sloped gas layers proportional to $\mathrm{Ra_L}^{1/3}$ for any slope in the range high values of H/L. Nusselt number hasn't show dependence on aspect ratio for high values (above 20). Natural convection and temperature profile in vertical layers have been investigated by Yin [40]. Collection of different models is accompanied with Niemann's correlations [41]. Selected equations are shown in *Tab. 2.3*.

Comparison of individual models is given in *Fig. 2.6*. Decreasing trend of Nusselt number with the slope of gas layer is commonly evident for variable Ra_L but there is not general agreement between individual correlations. For low Ra_L, Hollands and Buchberg show good agreement, for higher Ra_L by contrast models from Hollands and Schinkel agree in range of slope angles from 0 to 50°.

Author	**Equation**	**Ra_L**	**ϕ**	***H/L***
Hollands [36]	$Nu_L = 1+1.44\left[1-\frac{1708}{Ra_L \cos\phi}\right]^{+}\left(1-\frac{(\sin 1.8\phi)^{1.6}1708}{Ra_L\cos\phi}\right)+\left[\left(\frac{Ra_L\cos\phi}{5830}\right)^{1/3}-1\right]^{+}$	$0 < Ra_L < 10^5$	0°- 60°	cca 48
Buchberg [37]	for 3 ranges $Nu_L = 1+1.446\left(1-\frac{1708}{Ra_L\cos\phi}\right)^{+}$ $Nu_L = 0.229(Ra_L\cos\phi)^{0.252}$ $Nu_L = 0.157(Ra_L\cos\phi)^{0.285}$ for 2 ranges $Nu_L = 1+1.446\left(1-\frac{1708}{Ra_L\cos\phi}\right)^{+}$ $Nu_L = 0.157(Ra_L\cos\phi)^{0.285}$	$1708 < Ra_L\cos\phi < 5900$ $5900 < Ra_L\cos\phi < 9.2x10^4$ $9.2x10^4 < Ra_L\cos\phi < 10^6$ $1708 < Ra_L\cos\phi < 2500$ $2500 < Ra_L\cos\phi < 10^6$	0°- 60°	
Randall [38]	$Nu_L = 0.118\left[Ra_L\cos^2(\phi-45)\right]^{0.29}$	$2.8x10^3 < Ra_L < 2.2x10^5$	45°- 90°	9 - 36
Schinkel [39]	$Nu_L = a(\phi)Ra_L^{1/3}$ ϕ / $a(\phi)$: 0° 0.080; 10° 0.079; 20° 0.075; 30° 0.074; 40° 0.074; 50° 0.074; 60° 0.072; 70° 0.069; 80° 0.068; 90° 0.062	$10^5 < Ra_L < 4x10^6$	0° - 90°	6 - 27
Yin [40]	$Nu_L = 0.210Gr_L^{0.269}\left(\frac{H}{L}\right)^{-0.131}$	$1.5x10^3 < Gr_L < 7x10^6$	90°	5 - 79
Niemann [41]	$Nu_L = 1+\frac{m(Ra_L)^K}{Ra_L+n}$ ϕ / m / n / K: 0° 0.0700 $0.32x10^4$ 1.333; 45° 0.0430 $0.41x10^4$ 1.360; 90° 0.0236 $1.01x10^4$ 1.393	$10^2 < Ra_L < 10^8$		
superscript + indicates that content of brackets is considered only for positive values, for negative values the content is equal to 0. Function of superscript + can be arithmetically described by relation 0.5(X+|X|).				

Tab. 2.3 – Selected correlations for natural convection Nusselt number in the sloped closed gas layer (heat flow upward)

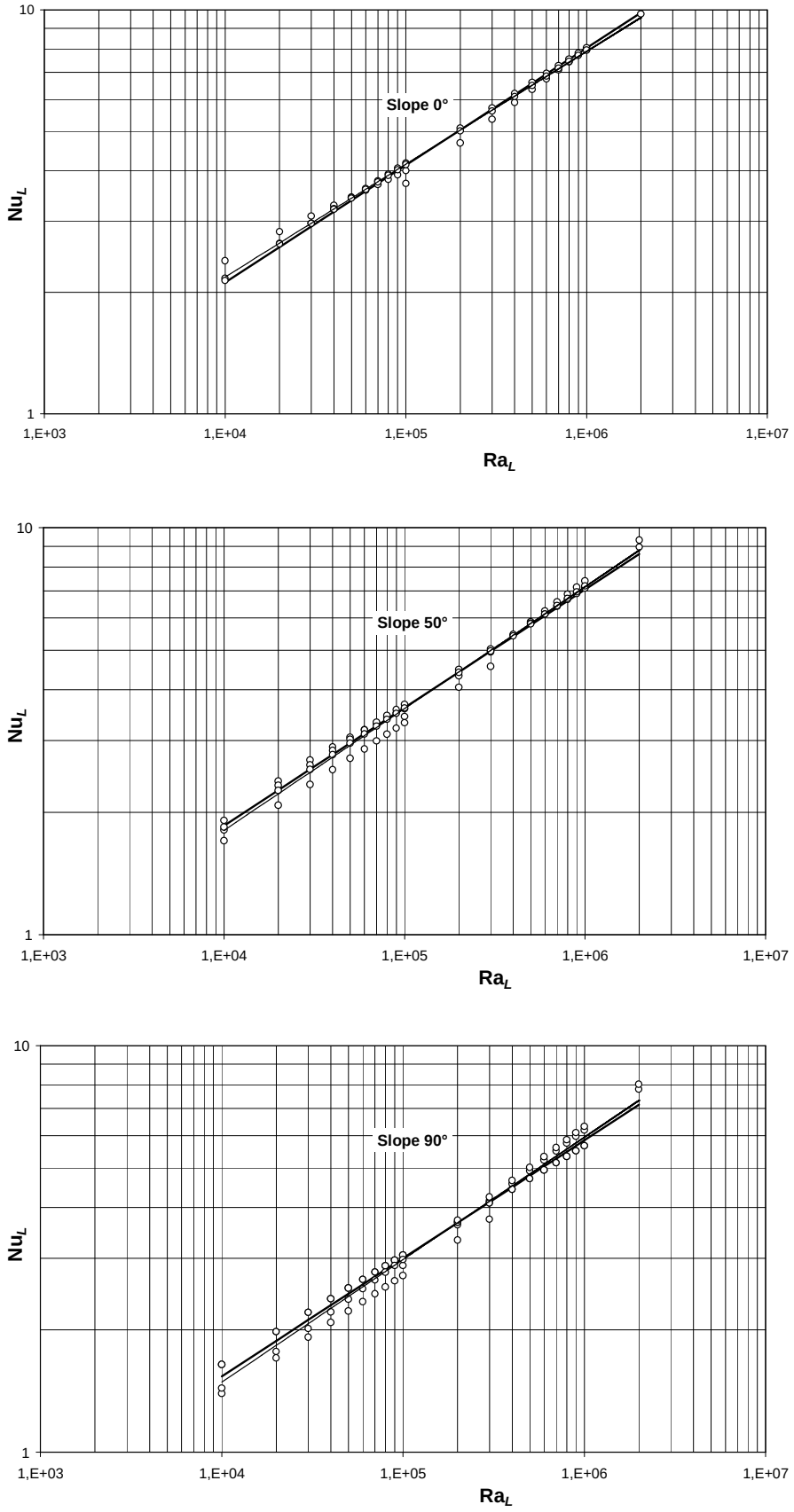

Fig. 2.5 – Nusselt numbers obtained from individual models and regression curve in the form of exponential A1-correlation $Nu_L = a.Ra_L^{0.29}$ (thick line) for different slopes of gas layer 0°, 50°a 90°

Application of only one from the offered models would limit possibility of modeling. Most of models are valid in certain range of slopes and cannot be applied for whole range from 0° to 90°. To overcome such limitation, the universal correlation (here called A1-correlation, see Equation 2.27) from given models has been derived by least squares method. Nusselt numbers given for Ra_L from 10^4 do 2×10^6 according to different authors has been put into graphs for individual air layer slopes (0°, 10°, 20°, ..., 90°). Exponential functions in the form

$$Nu_L = a(\phi)\, Ra_L^{0.29} \tag{2.25}$$

have been derived by the least squares method to get best fit of given values. Since Nusselt number is insensitive to aspect ratio at high values of *H/L,* the correlation hasn't concerned that problem. Slope angle dependence factor $a(\phi)$ has been obtained as polynomic function

$$a(\phi) = 0.1464 - 2.602\times10^{-4}\phi - 2.046\times10^{-6}\phi^2 \tag{2.26}$$

where

ϕ is slope angle, in deg.

Combining Equations (2.25) and (2.26) the complete form for A1-correlation is obtained

$$Nu_L = \left(0.1464 - 2.602\times10^{-4}\phi - 2.046\times10^{-6}\phi^2\right) Ra_L^{0.29}$$

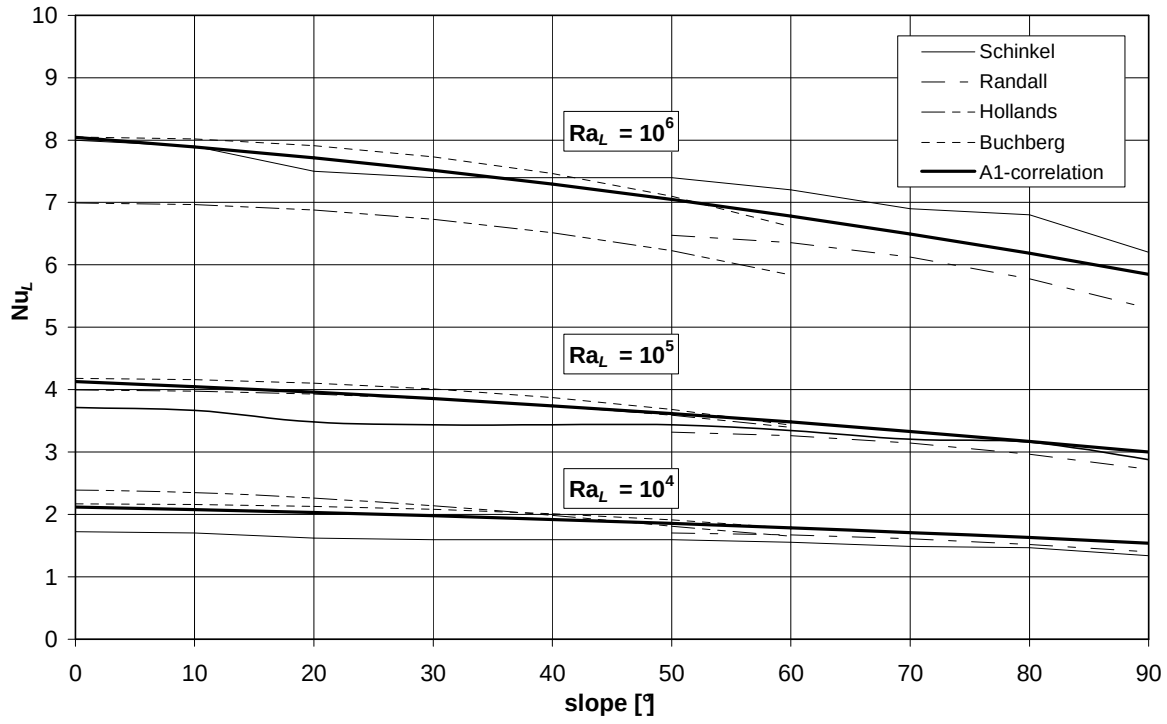

Fig. 2.6 – Comparison of different Nu_L models dependent on slope ϕ with the obtained A1-correlation for $Ra_L = 10^4$, $Ra_L = 10^5$ and $Ra_L = 10^6$

Fig. 2.6 shows a comparison of different models gained from literature review with obtained A1-correlation. Comparison is performed for different range of $Ra_L = 10^4$, 10^5 a 10^6.

2.3.7. Radiation between absorber and back frame ($h_{s,z2\text{-}abs}$)

Radiation heat transfer coefficient between back surface of absorber and interior surface of collector frame (back side of collector) is given by Stefan-Boltzman law similarly as in chapter 2.2.5

$$h_{s,z2-abs} = \frac{\sigma}{\frac{1}{\varepsilon_{z2}} + \frac{1}{\varepsilon_{abs,z}} - 1} \left(T_{abs}^2 + T_{z2}^2\right)\left(T_{abs} + T_{z2}\right) \qquad (2.28)$$

where

T_{z2} is frame interior surface temperature, in K;

T_{abs} absorber surface temperature, in K;

ε_{z2} emittance of frame interior surface;

$\varepsilon_{abs,z}$ emittance of back absorber surface.

Distinction between front and back absorber surface emittance is necessary since most of solar flat-plate collectors is equipped with spectrally selective coating at front absorber surface (low emittance in IR region) while back surface is left without any treatment (oxidized, dirty, etc.).

2.3.8. Natural convection between absorber and back frame ($h_{p,z2\text{-}abs}$)

Natural convection heat transfer coefficient in enclosed gas layer between absorber and interior surface of collector back frame is given by similar equation as in 2.2.6. Geometric parameters of gas layer and heat flow direction (downward) are outlined in *Fig. 2.7*.

$$h_{p,z2-abs} = \frac{Nu_L \lambda_g}{L_{z2-abs}} \qquad (2.29)$$

where

$L_{z2\text{-}abs}$ is thickness of gas layer between absorber and back frame, in m;

λ_g thermal conductivity of gas layer at mean temperature of layer $t_{z2\text{-}abs}$, in W/mK;

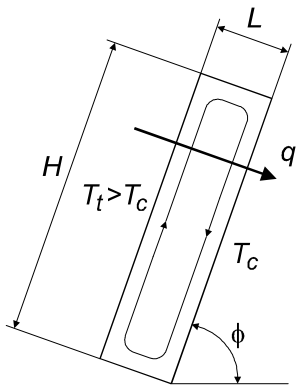

Fig.2.7 – Natural convection in enclosed gas layer (heat flow downward)

A literature review has been done to find proper equation for heat transfer coefficient for the case of natural convection in gas enclosure (closed gas layer) with heat flow downward required. Suitability of the equation application in area of solar collectors has been limited by following conditions:

- heat flow downward (slope angle range ϕ from 90° to 180°)
- high values of aspect ratio $H/L > 20$
- range of Ra_L from 10^4 to 2×10^6
- dependence of Nu_L on slope angle of gas layer ϕ, respectively on aspect ratio H/L

Only one general equation has been obtained. Arnold et al. [42] suggest correlation based on Nusselt number obtained for vertical gas layer (90°) as a sinus function in the range $90 < \phi < 180°$ as given in Equation (2.30)

$$Nu_L = 1 + [Nu_L(\phi = 90°) - 1]\sin\phi \tag{2.30}$$

Relationship is valid for range of Ra_L from 10^4 to 10^6 and for aspect ratio *H/L* above 12. In the mathematical model, the selection of the appropriate author means the selection of equation for $Nu_L(\phi = 90°)$ calculation and result for other slopes are calculated implicitly according to Arnold. *Fig. 2.8* shows a dependence of Nu_L on gas layer slope in the range from 0° to 180° for $Ra_L = 10^4$, 10^5, 10^6 with use of A1-correlation to obtain $Nu_L(90°)$.

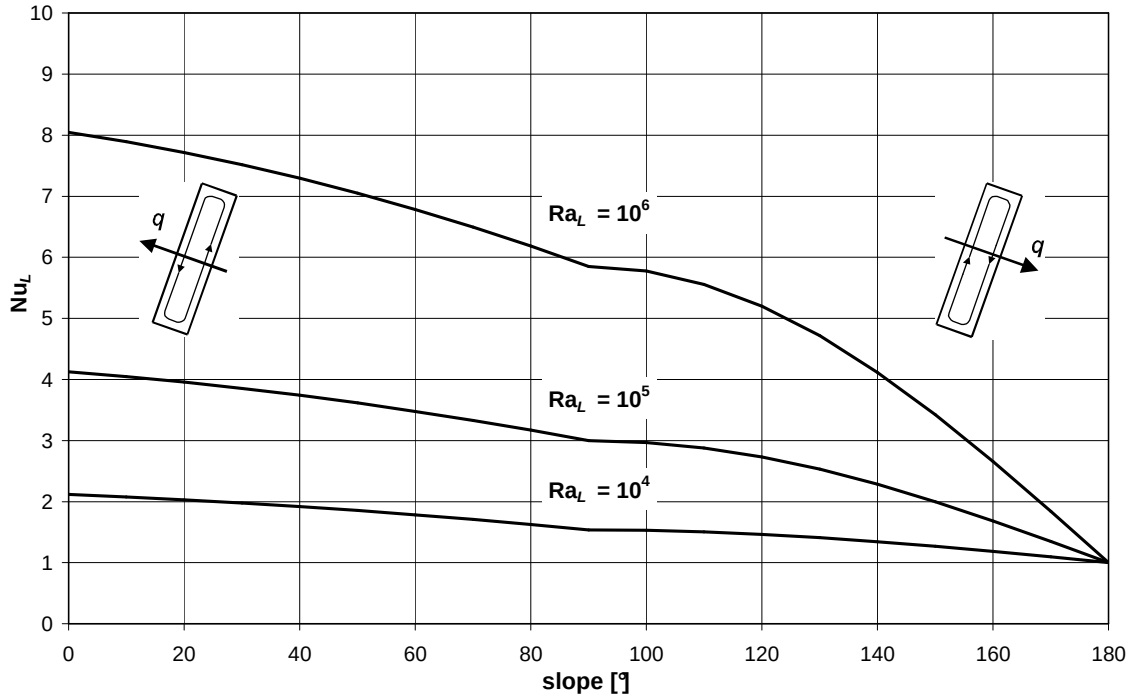

Fig. 2.8 Dependence of Nu_L for different Ra_L according to A1-correlation in complex range of gas layer slope angles

2.3.9. Conduction heat transfer through frame ($h_{v,z1\text{-}z2}$)

Thermal conductance of collector back frame (thermal insulation) is given by Equation (2.31)

$$h_{v,z1-z2} = \frac{\lambda_{z1-z2}}{L_{z1-z2}} \tag{2.31}$$

where

$\lambda_{z1\text{-}z2}$ is thermal conductivity of back frame material (mostly insulation), in W/mK;

$L_{z1\text{-}z2}$ thickness of back frame material, in m.

2.3.10. Radiation heat exchange between frame and adjacent ambient surfaces ($h_{s,z1\text{-}a}$)

Radiation heat transfer coefficient between exterior surface of collector back frame and adjacent surfaces in ambient environment (roof) related to ambient temperature T_a can be expressed as

$$h_{s,z1-a} = \sigma \frac{1}{\frac{1}{\varepsilon_{z1}} + \frac{1}{\varepsilon_{as}} - 1} \cdot \frac{T_{z1}^4 - T_{as}^4}{T_{z1} - T_a} \tag{2.32}$$

where

T_{z1} is absolute temperature of frame exterior surface, in K;

T_{as} absolute temperature of adjacent surface, in K;

T_a absolute ambient temperature, in K;

ε_{z1} emittance of frame exterior surface;

ε_{as} emittance of adjacent surface.

For most cases in ambient environment, T_{as} can be considered as equal to ambient temperature T_a. Equation (2.32) can be modified to

$$h_{s,z1-a} = \frac{\sigma}{\frac{1}{\varepsilon_{z1}} + \frac{1}{\varepsilon_{as}} - 1} \left(T_{z1}^2 + T_a^2\right)\left(T_{z1} + T_a\right) \tag{2.33}$$

2.3.11. Wind convection heat transfer from back frame to ambient ($h_{p,z1\text{-}a}$)

Wind convection heat transfer coefficient from back side of collector frame to ambient can be determined similarly to 2.2.3.

2.3.12. Collector heat loss coefficient (*U*-value)

As illustrated in *Fig. 2.2*, heat loss coefficient for front side of the collector U_p can be determined as

$$U_p = \frac{1}{\frac{1}{h_{s,p1-a} + h_{p,p1-a}} + \frac{1}{h_{v,p1-p2}} + \frac{1}{h_{s,abs-p2} + h_{p,abs-p2}}} \tag{2.34}$$

By analogy, heat loss coefficient for back side of the collector U_z can be determined as

$$U_z = \frac{1}{\frac{1}{h_{s,z1-a} + h_{p,z1-a}} + \frac{1}{h_{v,z1-z2}} + \frac{1}{h_{s,abs-z2} + h_{p,abs-z2}}} \tag{2.35}$$

Heat transfer coefficients for edge side of the collector frame can be determined in similar way as for the back side[4].

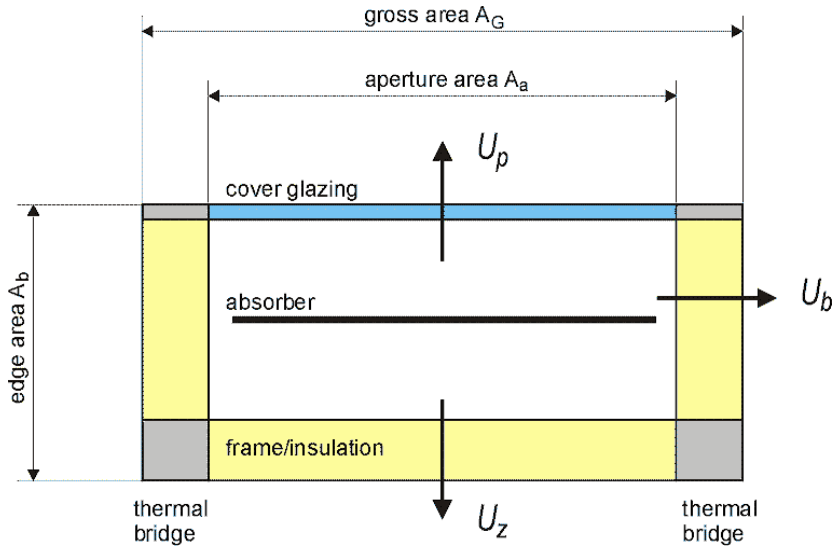

Fig. 2.9 – Collector heat loss with respect to aperture and gross area

Overall heat loss of solar collector (*U*-value) is related to gross dimensions (gross collector area A_G) as illustrated in *Fig. 2.9* to cover the effect of thermal bridges not to underestimate the heat loss. On the other side, the usable heat output of the collector refers to aperture area A_a, therefore overall collector heat loss coefficient *U* used in the internal energy balance calculations should be also related to aperture area A_a. From the balance of specific heat loss

$$U_G A_G = U_p A_G + U_z A_G + U_b A_b = U A_a \tag{2.36}$$

the overall heat loss coefficient *U* based on aperture area can be obtain as

$$U = \left(U_p + U_z + U_z \frac{A_b}{A_G} \right) \frac{A_G}{A_a} \tag{2.37}$$

2.4. Internal energy balance of the absorber

Heat transfer from absorber surface to liquid flowing through the pipe register of absorber can be described by internal energy balance of the absorber. Theoretical calculation is based on solving the temperature distribution on the absorber fin (well known analytical solution of fin efficiency, but irradiated by sun), i.e. differential equation of second order with two boundary conditions and the temperature gradient along the pipe [1]. Schematic outline of absorber balance and temperature profile at the fin cross section is shown in *Fig. 2.10*.

[4] Model KOLEKTOR 2.2 simplifies the calculation and heat loss coefficient for edge side U_b is considered the same as for back side U_z. Next version of KOLEKTOR 3.1 will handle U_b and U_z separately.

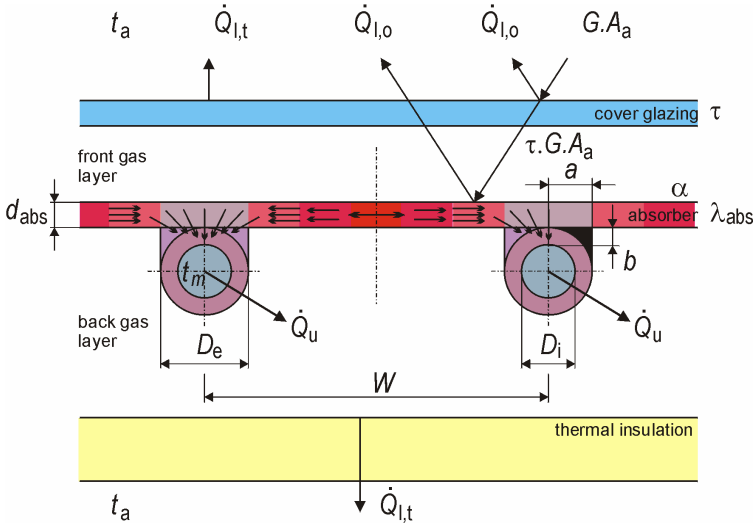

Obr. 2.10 – Schematic energy balance of solar collector with respect to internal absorber balance (fin and pipe configuration)

2.4.1. Fin efficiency *F*

When considered absorber element as a fin, it is convenient to introduce the concept of fin efficiency given by Equation (2.38)

$$F = \frac{\tanh[m(W - D_e)/2]}{m(W - D_e)/2} \tag{2.38}$$

where

$$m = \sqrt{\frac{U}{\lambda_{abs} d_{abs}}} \tag{2.39}$$

with

W	is	fin length = distance between risers (axis to axis distance), in m;
D_e		external diameter of risers, in m;
λ_{abs}		thermal conductivity of absorber fin, in W/mK;
d_{abs}		thickness of the absorber fin, in m.

2.4.2. Collector efficiency factor *F'*

Except the conduction heat transfer by the fin, also conduction through the bond fin-pipe and heat transfer from pipe to liquid by forced convection influence the overall heat transfer from absorber surface to heat transfer liquid. The parameter describing how efficient is heat transfer form absorber surface to heat transfer fluid is called collector or absorber efficiency factor *F'*. It can be regarded as a ratio of two heat loss coefficients

$$F' = \frac{U_o}{U} \tag{2.40}$$

where

U_o	is	heat loss coefficient from liquid to ambient, in W/m^{2}K;

U solar collector heat loss coefficient from absorber to ambient, in W/m^{2}K.

Different absorber configurations (see *Fig. 2.11a-c*) result in appropriate equations. For upper bond of absorber to riser pipes the efficiency factor is given as

$$F' = \frac{1/U}{W\left[\frac{1}{U[D_e + (W - D_e)F]} + \frac{1}{C_{sp}} + \frac{1}{h_i \pi D_i}\right]} \tag{2.41a}$$

where

C_{sp} is bond thermal conductance, in W/mK;

D_i internal diameter of riser pipe, in m;

h_i forced convection heat transfer coefficient in riser pipe, in W/m^{2}K.

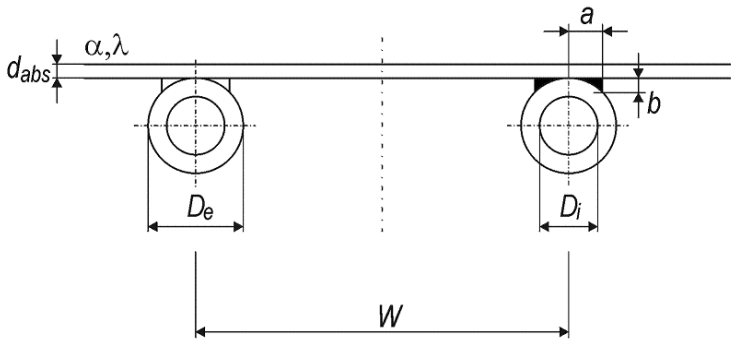

Fig. 2.11a – Absorber–pipe upper bond configuration

For side bond of absorber to riser pipes the efficiency factor is given as

$$F' = \frac{1/U}{W\left[\frac{1}{U[D_e + (W - D_e)F]} + \frac{1}{h_i \pi D_i}\right]} \tag{2.41b}$$

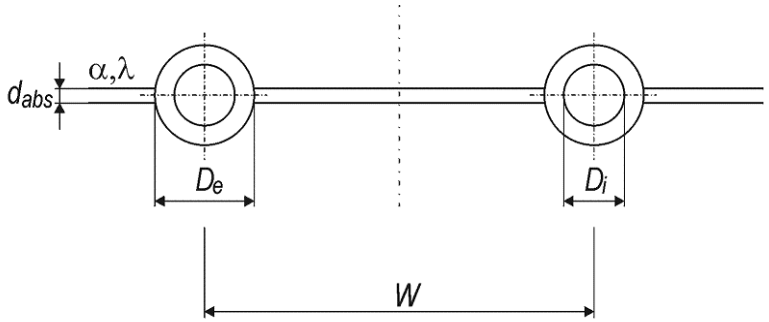

Fig. 2.11b – Absorber–pipe side bond configuration

For lower bond of absorber to riser pipes the efficiency factor is given as

$$F' = \frac{1}{\frac{WU}{h_i \pi D_i} + \frac{1}{\frac{D_e}{W} + \frac{1}{\frac{WU}{C_{sp}} + \frac{W}{(W - D_e)F}}}} \tag{2.41c}$$

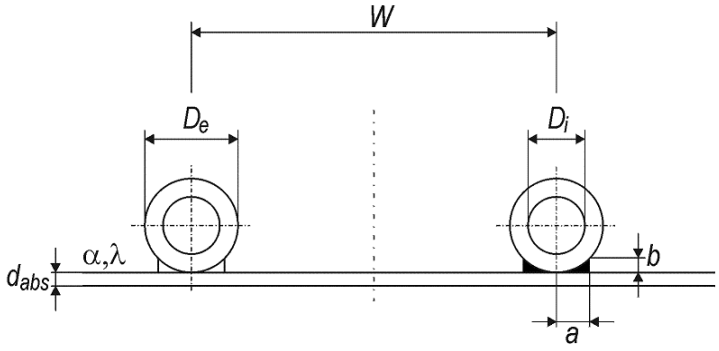

Fig. 2.11 – Absorber–pipe lower bond configuration

2.4.3. Bond thermal conductance C_{sp}

Bond thermal conductance C_{sp} is estimated from Equation (2.42) as given

$$C_{sp} = \frac{\lambda_{sp}\, a}{b} \tag{2.42}$$

where

λ_{sp} is bond thermal conductivity, in W/mK;

a average bond width, in m;

b average bond thickness, in m.

Bond thermal conductance could not be easily estimated especially for imperfect bonds (e.g. clamping bond). As good metal-to-metal contact can be regarded if bond thermal conductance is greater than 30 W/mK. Very poor contacts (clamps, slight touch, etc.) result in values less than 10 W/mK.

2.4.4. Forced convection heat transfer in pipes (h_i)

Forced convection heat transfer coefficient between the fluid and wall in absorber riser pipe is determined from Nusselt number

$$h_i = \mathrm{Nu}_D \cdot \frac{\lambda_f}{D_i} \tag{2.43}$$

where

λ_f is thermal conductivity of heat transfer fluid, in W/mK;

D_i internal diameter of riser pipes, in m.

Laminar forced convection heat transfer in circular pipes is widely described in [50, 51]. *Tab. 2.4* shows correlations for Nusselt number for laminar forced convection heat transfer found in literature. The case of constant heat flux shows higher

applicability (riser pipe is uniformly irradiated) than constant temperature case (temperature varies along riser length in solar collector).

Other boundary conditions can be taken into account as developing profiles of temperature or velocity. For developing flow, dimensionless longitudinal coordinate x^* is defined as inverse value of Graetz number characterizing the laminar flow in pipes as given in Equation (2.44)

$$x^* = \mathrm{Gz}^{-1} = \frac{x / D_\mathrm{i}}{\mathrm{Re_D} \cdot \mathrm{Pr}} \tag{2.44}$$

where riser pipe length L [m] is used for the coordinate x.

Author	Equation	Conditions
Fully developed region		
Shah [50]	$\mathrm{Nu_D} = \frac{48}{11} = 4.364$	constant heat flux
	$\mathrm{Nu_D} = 3.657$	constant temperature
Entry region - thermally developing flow thermal entry length / developed velocity profile, developing temp. profile (thermally developing Hagen-Poiseuille flow)		
Shah [50]	$\mathrm{Nu_D} = \begin{cases} 1.615\, x^{*-1/3} - 0.7 & x^* \le 0.005 \\ 1.615\, x^{*-1/3} - 0.2 & 0.005 < x^* < 0.03 \\ 3.657 + \frac{0.0499}{x^*} & x^* \ge 0.03 \end{cases}$	constant surface temperature
	$\mathrm{Nu_D} = \begin{cases} 1.953\, x^{*-1/3} & x^* \le 0.03 \\ 4.364 + \frac{0.0722}{x^*} & x^* > 0.03 \end{cases}$	constant heat flux
Hausen [46]	$\mathrm{Nu_D} = 3.66 + \frac{0.19\left[(D/L)\,\mathrm{Re_D Pr}\right]^{0.8}}{1 + 0.117\left[(D/L)\,\mathrm{Re_D Pr}\right]^{0.467}}$	constant temperature
Hausen [52]	$\mathrm{Nu_D} = 3.66 + \frac{0.0668\,(D/L)\,\mathrm{Re_D Pr}}{1 + 0.04\left[(D/L)\,\mathrm{Re_D Pr}\right]^{2/3}}$	
Entry region - thermally and hydraulically developing flow combined entry length, simultaneously developing flow, velocity and temperature profiles developing together		
Kreith, Kays [51]	$\mathrm{Nu_D} = \frac{1}{4x^*} \ln\left(\frac{1}{1 - 2.654\, x^{*0.5}\, \mathrm{Pr}^{-0.167}}\right)$	constant wall temperature Pr > 2 $10^{-7} \le x^* \le 10^{-3}$
Churchill and Ozoe	$\mathrm{Nu_D} = \frac{2 \cdot 0.6366\left[(4/\pi)\, x^*\right]^{-1/2}}{\left[1 + (\mathrm{Pr}/0.0468)^{2/3}\right]^{1/4}}$	Pr > 2 $10^{-7} \le x^* \le 10^{-3}$
Sieder-Tate [53]	$\mathrm{Nu_D} = 1.86\left(\frac{\mathrm{Re_D \cdot Pr}}{L/D}\right)^{1/3}\left(\frac{\mu}{\mu_\mathrm{w}}\right)^{0.14}$	constant temperature 0.48 < Pr < 16700 $0.0044 < \left(\frac{\mu}{\mu_\mathrm{w}}\right) < 9.75$ recommended for $\left(\frac{\mathrm{Re_D \cdot Pr}}{L/D}\right)^{1/3} \cdot \left(\frac{\mu}{\mu_\mathrm{w}}\right)^{0.14} > 2$ else fully developed profile

Tab. 2.4 – Correlations for laminar forced convection heat transfer in pipes

In the case of turbulent flow, different set of equations (see *Tab. 2.5*) is applicable to calculation of the Nusselt number, mostly in the form

$$\mathrm{Nu_D} = A\,\mathrm{Re_D^{\,m}}\,\mathrm{Pr}^{n} \qquad (2.45)$$

or based on friction factor *f* of pipes.

The turbulent flow inside the riser pipes of solar collectors is very rare when using antifreeze water-glycol mixtures as heat transfer fluid with high viscosity.

Author	Equation	Conditions
Fully developed region		
Colburn [55]	$\mathrm{Nu_D} = 0.023\,\mathrm{Re_D^{4/5}}\,\mathrm{Pr}^{1/3}$	$2\times10^4 < \mathrm{Re_D} < 10^6$
Dittus-Boelter [56]	$\mathrm{Nu_D} = 0.023\,\mathrm{Re_D^{4/5}}\,\mathrm{Pr}^{n}$ n = 0.4 for heating ($T_w > T_m$), n = 0.3 for cooling ($T_w < T_m$)	$0.7 \le \mathrm{Pr} \le 120$ $2500 \le \mathrm{Re_D} \le 1.24\times10^5$ $L/D > 60$
Dittus-Boelter interpreted by Kakac [59]	$\mathrm{Nu_D} = 0.023\,\mathrm{Re_D^{4/5}}\,\mathrm{Pr}^{0.4}$ $\mathrm{Nu_D} = 0.026\,\mathrm{Re_D^{4/5}}\,\mathrm{Pr}^{0.4}$	for heating for cooling
Sieder-Tate [53]	$\mathrm{Nu_D} = 0.027\,\mathrm{Re_D^{4/5}}\,\mathrm{Pr}^{1/3}\left(\frac{\mu}{\mu_w}\right)^{0.14}$	modification of Coburn $0.7 \le \mathrm{Pr} \le 16700$ $10^4 \le \mathrm{Re_D}$
Petukhov-Kirillov-Popov [57]	$\mathrm{Nu_D} = \frac{(f/8)\,\mathrm{Re_D}\,\mathrm{Pr}}{1.07+12.7\,(f/8)^{1/2}\left(\mathrm{Pr}^{2/3}-1\right)}$ friction factor according Moody diagram smooth pipes $f = (1.82\log_{10}\mathrm{Re_D} - 1.64)^{-2}$	$0.5 < \mathrm{Pr} < 2000$ $10^4 < \mathrm{Re_D} < 5\times10^6$
Gnielinski [58]	$\mathrm{Nu_D} = \frac{(f/8)\,(\mathrm{Re_D}-1000)\,\mathrm{Pr}}{1+12.7\,(f/8)^{1/2}\left(\mathrm{Pr}^{2/3}-1\right)}$ smooth pipes $f = (0.79\ln\mathrm{Re_D} - 1.64)^{-2}$	$0.5 < \mathrm{Pr} < 2000$ $2300 < \mathrm{Re_D} < 5\times10^6$
Hausen	$\mathrm{Nu_D} = 0.037\left[1+\left(\frac{D}{L}\right)^{2/3}\right]\left(\mathrm{Re_D^{0.75}}-180\right)\mathrm{Pr}^{0.42}\left(\frac{\mu}{\mu_w}\right)^{0.14}$	$0.6 < \mathrm{Pr} < 10^3$ $2300 < \mathrm{Re_D} < 10^6$ $1 < D/L < 0$ μ_w for wall temperature (T_w), μ for T_m (mean fluid temperature)
Sleicher, Rouse [49]	$\mathrm{Nu_D} = 5 + 0.015\,\mathrm{Re_D^{\,a}}\,\mathrm{Pr}^{b}$ $a = 0.88 - \frac{0.24}{4+\mathrm{Pr}} \qquad b = 0.333 + 0.5e^{-0.6\mathrm{Pr}}$	$0.1 < \mathrm{Pr} < 10^4$ $10^4 < \mathrm{Re} < 10^6$
Jacob	$\mathrm{Nu_D} = 0.036\,\mathrm{Re_D^{0.8}}\,\mathrm{Pr}^{1/3}\left(\frac{\mu}{\mu_w}\right)^{0.14}\left(\frac{D}{L}\right)^{1/18}$	

Tab. 2.5 – Correlations for turbulent forced convection heat transfer in pipes

2.4.5. Collector heat removal factor F_R

Energy balance of the fluid flowing through the riser pipe element can be described by differential equation. Solution results in fluid temperature distribution along riser pipe coordinate in flow direction [1, 12].

Collector heat removal factor F_R is defined as actual useful energy gain of collector to useful gain if the absorber surface was at the fluid temperature. By introduction of fluid temperature distribution the heat removal factor can be expressed as

$$F_R = \frac{\dot{M}c}{A_a U}\left[1 - \exp\left(-\frac{A_a U F'}{\dot{M}c}\right)\right] \tag{2.46}$$

where

$\dot{M}$ is total mass flow rate of fluid through solar collector, in kg/s;

c_f specific thermal capacity of fluid, in J/kgK;

A_a aperture area of solar collector, in m^2.

Collector heat removal factor F_R is equivalent to the effectiveness of a conventional heat exchanger, which is defined as ratio of the actual heat transfer to the maximum possible heat transfer. Maximum possible useful heat gain in a solar collector occurs when the whole absorber is at the inlet fluid temperature (no temperature increase along the riser pipes, minimized heat loss) [1].

2.4.6. Useful heat output of solar collector

Useful thermal output from solar collector can be defined in three different ways, based on given reference collector temperature. From external balance of absorber, the usable thermal power output results as

$$\dot{Q}_u = A_a[(\tau\alpha)_{ef} G - U(t_{abs} - t_a)] \tag{2.47}$$

where

$(\tau\alpha)_{ef}$ is effective product of transmittance of cover glazing and absorptance of absorber;

U collector heat loss coefficient related to aperture area, in W/m^{2}K;

G solar irradiation incident on aperture, in W/m^2;

A_a aperture area of solar collector, in m^2.

The evaluation of thermal power output based on mean absorber temperature t_{abs} is not very practical due to difficulty of identifying t_{abs} by experimental measurements.

Expressing the thermal power output based on mean fluid temperature t_m is more practical, because it corresponds with results from experimental testing of solar collectors. Mean fluid temperature can be easily obtained from measured input and output temperatures as

$$t_m = \frac{t_{in} + t_{out}}{2} \tag{2.48}$$

where

t_{in} is collector input temperature, in ℃;

t_{out} collector output temperature, in ℃.

Usable thermal power output from collector based on mean fluid temperature is defined by introduction of efficiency factor F' as

$$\dot{Q}_u = A_a F'[(\tau\alpha)_{ef} G - U(t_m - t_a)] \quad (2.49)$$

For mathematical modeling of solar systems, calculation of heat output and output temperature from collector based on input temperature is needed[5]. Usable heat output based on input temperature can be given as

$$\dot{Q}_u = A_a F_R[(\tau\alpha)_{ef} G - U(t_{in} - t_a)] \quad (2.50)$$

2.4.7. Efficiency of solar collector

Collector efficiency is defined as usable thermal power output from the collector related to solar radiation input incident on front part of collector (defined by reference collector area = aperture area A_a). Similarly to usable thermal power output of collector, also efficiency can be related to

mean absorber temperature $$\eta = (\tau\alpha)_{ef} - U\frac{(t_{abs} - t_a)}{G} \quad (2.51)$$

mean fluid temperature $$\eta = F'\left[(\tau\alpha)_{ef} - U\frac{(t_m - t_a)}{G}\right] \quad (2.52)$$

fluid input temperature $$\eta = F_R\left[(\tau\alpha)_{ef} - U\frac{(t_{in} - t_a)}{G}\right] \quad (2.53)$$

The last equation is a basic relationship in solar thermal collector theory, so called ***Hottel-Whilier-Bliss*** solar collector efficiency equation.

2.4.8. Fluid and absorber temperature

To calculate heat transfer coefficients at main surfaces of solar collector and to assess the overall collector heat loss coefficient U (external energy balance) the absorber temperature should be identified from input temperature as given in Equation (2.54)

$$t_{abs} = t_{in} + \frac{\dot{Q}_u / A_a}{F_R U}(1 - F_R) \quad (2.54)$$

It is apparent that mutual dependence of t_{abs} and U results in iteration calculation loop (see chapter 2.4).

Mean fluid temperature t_m necessary for calculation of convection heat transfer coefficient h_i for fluid in pipes can be obtained from input temperature as given in Equation (2.55)

$$t_m = t_{in} + \frac{\dot{Q}_u / A_a}{F_R U}\left(1 - \frac{F_R}{F'}\right) \quad (2.55)$$

[5] Such expression of collector thermal power output is used in mathematical model KOLEKTOR, since the calculation is based on input temperature.

The calculation of temperatures is processed in superior iteration loop since external and internal energy balances are mutually dependent.

2.5. Iteration process

2.5.1. External energy balance

The core of the external energy absorber balance is an iteration loop for calculation of temperature distribution for main surfaces (temperature levels) of solar collector. At the start of iteration process, absorber temperature is estimated from input fluid temperature, generally as

$$t_{\mathrm{abs}} = t_{\mathrm{in}} + 10\ \mathrm{K} \tag{2.56}$$

To calculate heat transfer coefficients between main collector surfaces (p1, p2, z1, z2), the surface temperatures are needed but at the start of calculation process the temperatures are not known. In the first iteration step, surface temperatures are estimated from temperature difference between absorber and ambient environment uniformly as follows

$$t_{\mathrm{p1}} = t_{\mathrm{z1}} = t_{\mathrm{abs}} - \frac{t_{\mathrm{abs}} - t_{\mathrm{a}}}{3} \tag{2.57}$$

$$t_{\mathrm{p2}} = t_{\mathrm{z2}} = t_{\mathrm{a}} + \frac{t_{\mathrm{abs}} - t_{\mathrm{a}}}{3} \tag{2.58}$$

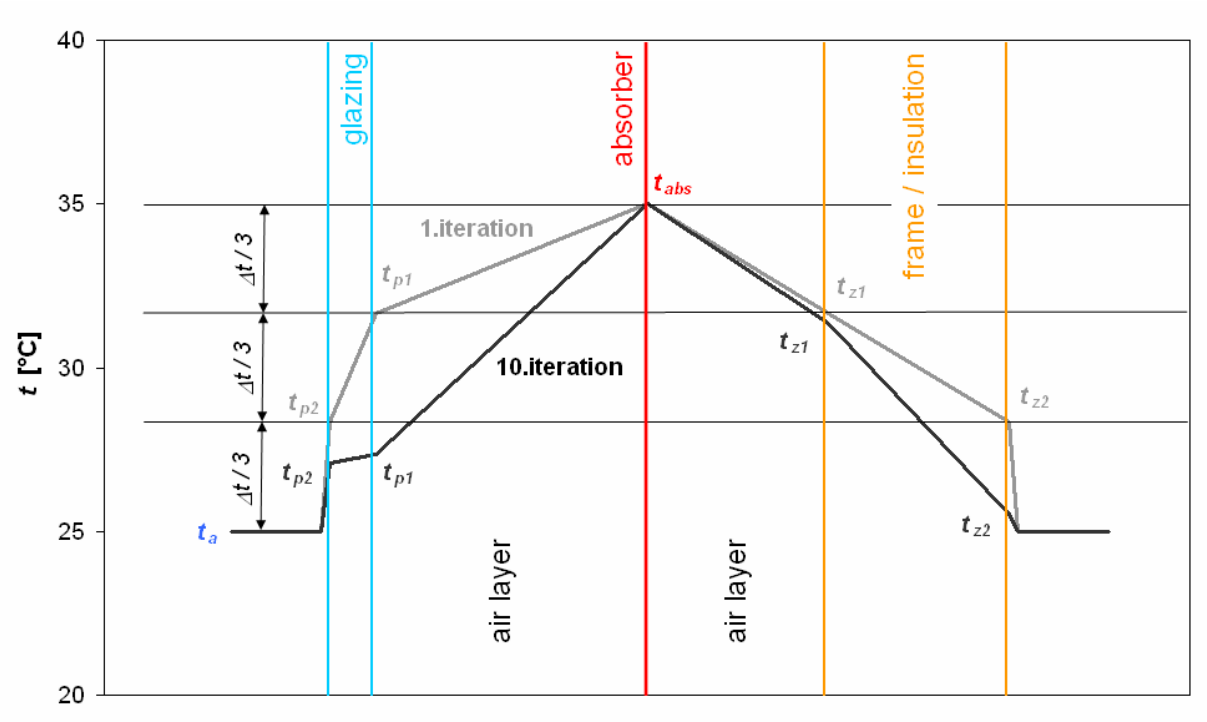

Fig. 2.12 – Temperature distribution in collector at the start and the end of iteration process of external energy balance of absorber

After that heat transfer coefficients can be calculated and collector heat loss coefficients U_{p} and U_{z} can be obtained. Since these coefficients have been calculated for incorrect temperatures, next iteration step should follow. From heat transfer coefficients and heat flows through front and back side of collector

temperature distribution can be obtained by reverse calculation process. For given absorber temperature t_{abs} and ambient temperature t_a, heat flow from absorber to ambient, here for the front side, is given as

$$q_p = U_p\left(t_{abs} - t_a\right) \tag{2.59a}$$

$$q_p = \left(h_{s,abs-p1} + h_{p,abs-p1}\right)\left(t_{abs} - t_{p1}\right) \tag{2.59b}$$

$$q_p = h_{v,p1-p2}\left(t_{p1} - t_{p2}\right) \tag{2.59c}$$

$$q_p = \left(h_{s,p2-a} + h_{p,p2-a}\right)\left(t_{p2} - t_a\right) \tag{2.59d}$$

Combining the Equations (2.59a) to (2.59d), the main surface temperatures for next iteration step can be obtained as

$$t_{p1} = t_{abs} - \frac{U_p}{\left(h_{s,abs-p1} + h_{p,abs-p1}\right)}\left(t_{abs} - t_a\right) \tag{2.60}$$

$$t_{p2} = t_a + \frac{U_p}{\left(h_{s,p2-a} + h_{p,p2-a}\right)}\left(t_{abs} - t_a\right) \tag{2.61}$$

Analogous to front side surface temperatures calculation, for back side can be applied

$$t_{z1} = t_{abs} - \frac{U_z}{\left(h_{s,abs-z1} + h_{p,abs-z1}\right)}\left(t_{abs} - t_a\right) \tag{2.62}$$

$$t_{z2} = t_a + \frac{U_z}{\left(h_{s,z2-a} + h_{p,z2-a}\right)}\left(t_{abs} - t_a\right) \tag{2.63}$$

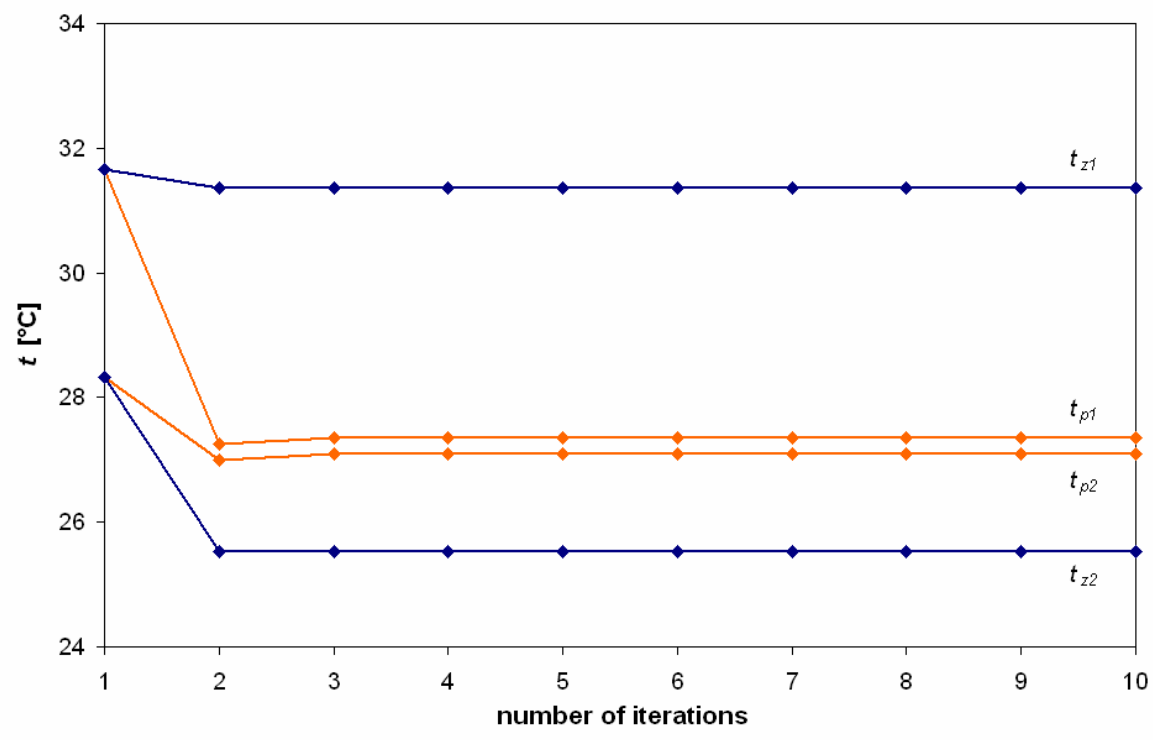

Fig. 2.13 – Values of calculated temperatures during iteration process

The new and more correct values of surface temperatures are used in next iteration step for calculation of individual heat transfer coefficients between the surfaces and new and more correct value of heat loss coefficient *U* (see *Fig. 2.12*). Iteration process converges very quickly, the temperature distribution becomes stable and external energy balance is finished after 5 iterations as illustrated in *Fig. 2.13*.

2.5.2. Internal energy balance

Internal energy absorber balance is processed in simple iteration loop for calculation of correct mean fluid temperature. At the start of iteration process, mean fluid temperature t_m is estimated from input fluid temperature

$$t_m = t_{in} + 10\ \mathrm{K} \tag{2.64}$$

Based on estimated mean fluid temperature, internal balance calculations are performed and new value of mean fluid temperature is obtained from Equation (2.55) for next iteration step. Analogous to external balance, the iteration process comes quickly to stable phase with no additional change in mean fluid temperature. Except the usable thermal power $\dot{Q}_u$ and efficiency of solar collector one of the main outputs of internal balance is the absorber temperature t_{abs}.

2.5.3. Superior iteration loop

Both external and internal energy balances are mutually dependent. Overall collector heat loss coefficient *U* as main output from external balance is one of the inputs for internal balance. On the other side, mean absorber temperature t_{abs} as one of the outputs from internal balance is used as necessary input for external balance. Superior iteration loop has been introduced to transfer the results from finished external balance iteration loop to starting cycle of internal balance iteration loop and results from finished internal balance iteration loop are put to first cycle of external balance loop. The scheme of iteration loops is outlined in *Fig. 2.14*.

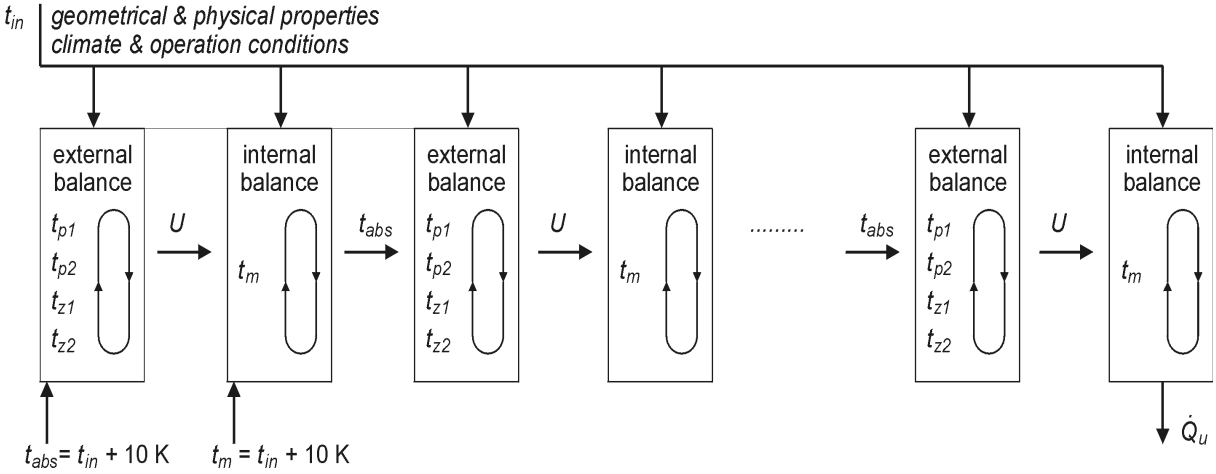

Fig. 2.14 – Scheme of iteration loops

2.6. Special features

2.6.1. Heat transfer fluids models

Mathematical models describing the thermal properties of heat transfer fluids (water, water-etyleneglycol solution, water-propyleneglycol solution) have been taken from [60]. Properties for pure water can be obtained from models when glycol mass concentration ξ is equal to zero. Below, the polynomic functions describing individual properties dependent on temperature are shown and appropriate constants are listed in *Tab. 2.6* and *Tab. 2.7*.

Freezing temperature T_F [K] of water-glycol solution may be determined by an equation of the form

$$\frac{T_F}{273.15} = A_0 + A_1\xi + A_2\xi^2 \tag{2.65}$$

where

ξ is mass concentration of glycol in aqueous solution

The density ρ, thermal conductivity λ and specific thermal capacity c may be all calculated by the same kind of equation. The property is here represented by P_x

$$P_x = A_1 + A_2\xi + A_3\frac{273.15}{T} + A_4\xi\frac{273.15}{T} + A_5\left(\frac{273.15}{T}\right)^2 \tag{2.66}$$

The same applies to the calculation of the dynamic viscosity μ and Prandtl number Pr, with slightly different equation

$$\ln(P_x) = A_1 + A_2\xi + A_3\frac{273.15}{T} + A_4\xi\frac{273.15}{T} + A_5\left(\frac{273.15}{T}\right)^2 \tag{2.67}$$

Parameter A order	ρ [kg/m^3]	c [kJ/kg.K]	λ [W/m.K]	μ [Pa.s]	Pr [-]	T_F [K]
0	-	-	-	-	-	1.0
1	658.49825	5.36449	0.83818	-4.63024	3.96951	-0.06982
2	-54.81501	0.78863	-1.37620	-2.14817	0.70076	-0.35780
3	664.71643	-2.59001	-0.07629	-12.70106	-12.98045	-
4	232.72605	-2.73187	1.07720	5.40536	2.64789	-
5	-322.61661	1.43759	-0.20174	10.98990	11.58900	-

Tab. 2.6 – Parameters of the mathematical models of aqueous solutions of ethyleneglycol [60]

Parameter *A* order	ρ [kg/m^3]	c [kJ/kg.K]	λ [W/m.K]	μ [Pa.s]	Pr [-]	T_F [K]
0	-	-	-	-	-	1.0
1	508.41109	4.47642	1.18886	-1.02798	6.66139	-0.03736
2	-182.40820	0.60863	-1.49110	-10.03298	-6.99440	-0.40050
3	965.76507	-0.71497	-0.69682	-19.93497	-18.55114	-
4	280.29104	-1.93855	1.13633	14.65802	12.04640	-
5	-472.22510	0.47873	0.06735	14.62050	14.47735	-

Tab. 2.7 – Parameters of the mathematical models of aqueous solutions of propyleneglycol [60]

2.6.2. Building integration

Sparrow et al. [64, 65] carried out a number of experiments to investigate local heat transfer coefficients on heated plates (e.g. solar collectors) under airflow at different conditions (angles of inclination of the plate relative to oncoming airstream, different velocities, framing surfaces). It was realized that average convection heat transfer coefficients are practically independent of the incident angle of airstream.

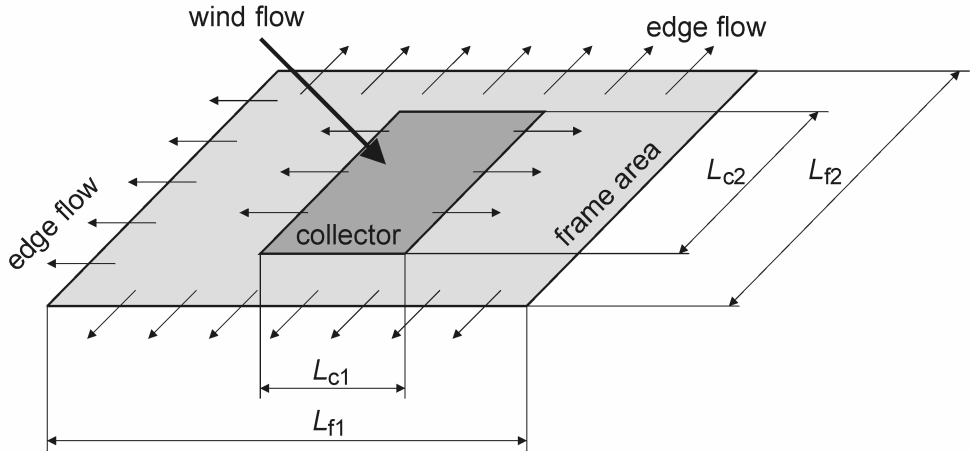

Fig. 2.15 – Oncoming wind airstream to collector integrated to thermally inactive frame

From the airflow patterns on the plate, a considerable difference was found between the local heat transfer coefficients in the center of the plate and on the edges. Higher velocity on the edges leads to higher local heat transfer coefficients, while coefficients near the center are lower due airflow stagnation. Average convection heat transfer coefficients can be substantially reduced when a thermally active surface (solar collector) is framed by another thermally inactive surface (the envelope surface). This result is important for the case of constructional integration of solar collectors into building envelope. Sparrow [65] gives an equation to obtain the rate of reduction of an average wind convection heat transfer coefficient

$$h_{w,int} = h_w \sqrt{\frac{L_c}{L_f}} \tag{2.68}$$

where $h_{w,int}$ and h_w respectively denote the coefficients in the presence of the frame (envelope integration) and in the absence of the frame (separate installation). The hydrodynamic dimensions L_c (solar collector) and L_f (envelope framing surface) are determined as characteristic lengths from

$$L = \frac{2L_1L_2}{L_1 + L_2} \tag{2.69}$$

In the example shown in *Fig. 2.16* solar collector located at flat roof and second one integrated into building facade will result in different values of wind-related heat transfer coefficients. While the average heat transfer coefficient at the glazing surface of a roof collector corresponds to wind velocity, the average heat transfer coefficient at the surface of a façade collector is lower due to the framing effect. For an investigated case of a common block of flats, the wind-related coefficient can be reduced to 60-80 % of the value for a roof located collector.

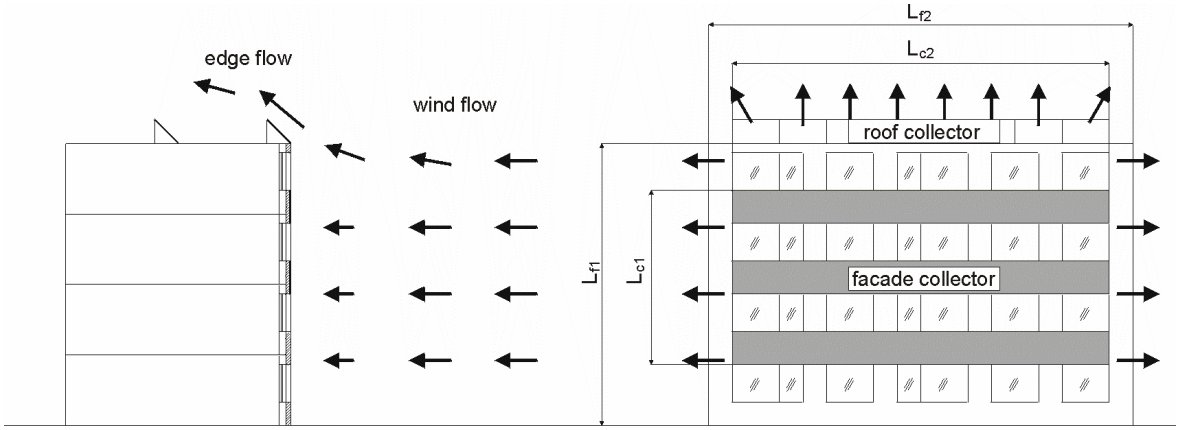

Fig. 2.16 - Wind flow over a building with solar collectors

2.6.3. Gas pressure inside collector

Evacuation of gas at constant temperature results in lower density of molecules $N_v = N/V$ in layer and the pressure p is reduced. The kinetic theory of gases relates gas viscosity coefficient μ to molecular diameter by

$$\mu = \frac{m_m}{3\sqrt{2}\pi d_m^2}\left(\frac{8kT}{\pi m_m}\right)^{1/2} \tag{2.70}$$

where

d_m is molecular diameter, in m.

m_m molecule mass, in atomic mass units (u).

According to the kinetic theory of gases, the gas dynamic viscosity μ is independent of gas pressure and increases with temperature.

Ideal gas law describes the state for a gas, as given in

$$pV = nRT \tag{2.71}$$

where

p	is	gas pressure, in Pa;
V		gas volume, in m^3;
n		number moles of gas, in mol;
R		ideal gas constant, 8.314 J/Kmol;
T		absolute temperature, in K.

Modification of ideal gas law with introducing molar mass [g/mol] $M = m / n$ and density [g/m^3] $\rho = m / V$ yields in

$$\rho = \frac{pM}{RT} \tag{2.72}$$

It is apparent that reducing the pressure will lower the gas density as mentioned above.

Due to evacuation of gas layer gas kinematic viscosity ν increases and natural convection in the gas layer is eliminated. So, Grashof number as a criterium describing the natural convection due to temperature difference decreases with pressure reduction as well as determined Nusselt number as a function of (Gr.Pr).

Free path of molecule defined as direct distance between two consequent collisions of gas molecule with other molecule increases with the decrease of pressure. Mean free path of molecule l_m is defined as arithmetical average of free paths of all molecules and is given by

$$l_m = \frac{kT}{\sqrt{2}\,\pi d_m^2 p} \tag{2.73}$$

where

k	is	Boltzmann constant, $1.380\,6504 \times 10^{-23}$ J/K;
T		absolute gas temperature, K;
p		pressure, in Pa;
d_m		diameter gas molecules, in m.

Mean free path l_m is inverse proportional to gas pressure p. Reduction of pressure leads also to decrease of mean frequency of molecule collisions which is determined by number of collisions of given molecule for a time period. This influences conduction heat transfer defined by frequency of molecule collisions.

The thermal conductivity of gas is virtually independent of pressure over many orders of magnitude. This curious property is the result of the almost exact inverse relationship between pressure and mean free path for molecule–molecule collisions. As the gas pressure is reduced, the number of gas molecules available to transport heat is reduced in proportion; however, the molecules travel correspondingly further between collisions.

With decrease of pressure below 100 Pa (medium vacuum) the mean free path of gas molecules l_m becomes comparable to the usual gas layer thickness in glazing or collector the heat is transferred through and thermal conductivity start to decrease.

For pressures under 0.1 Pa (high vacuum) the conduction heat transfer is realized only by molecules traveling from one boundary surface to other without any collisions (mean free path of molecules l_m > 10 mm).

Dependence of thermal conductivity of air λ on the air pressure between two surfaces is given by [61]

$$\lambda = \lambda_0 \frac{1}{1+\frac{7{,}6.10^{-5}}{p\frac{L}{T}}} \tag{2.74}$$

where

λ_0 is thermal conductivity at room temperature (20 °C), in W/mK.

L distance of layer boundary surfaces in heat flow direction, in m;

p pressure in air layer, in Pa;

T temperature, in K.

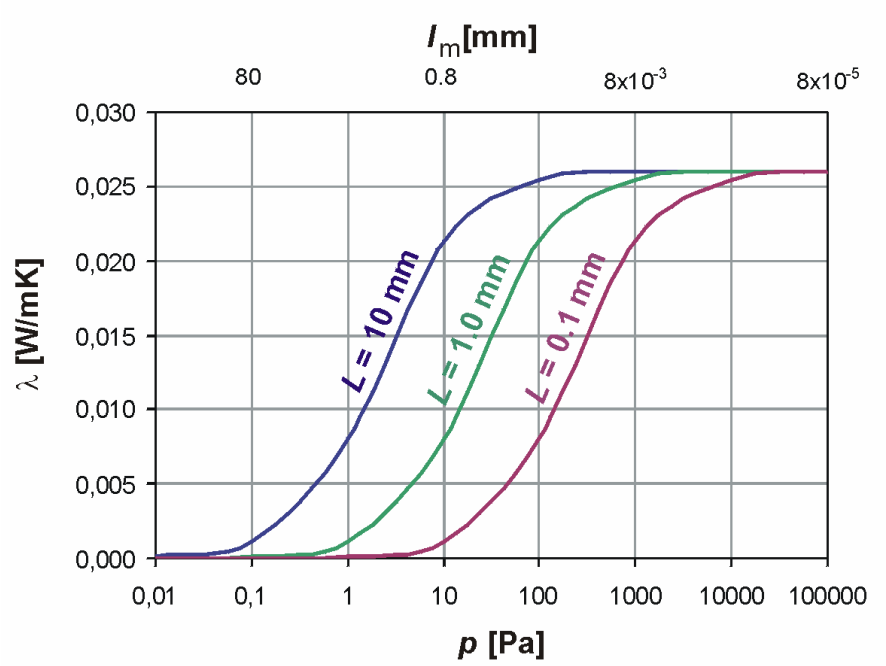

Fig. 2.17 – Dependence thermal conductivity vs. pressure, corresponding values of mean free path of air molecules (N_2) are given above (at 20 °C).

Fig. 2.17 shows the thermal conductivity is for given pressure lower for smaller size layer or cell size. Such effect is used preferably in vacuum insulations and evacuated aerogel structures. Smaller size of structure allows higher pressure to achieve required thermal resistance.

Further reduction in heat transport due to gaseous thermal conduction only occurs when the pressure is low enough that the mean free path for molecule–molecule collisions is of the same order as the distance over which the heat is transported. For vacuum glazing with a gap of 0.2 mm, this corresponds to a pressure of about 30 Pa. At lower pressures, the gaseous conductance [W/m^{2}K] is approximately proportional to pressure [62], and may be written as

$$\Lambda_g = \alpha\left(\frac{\gamma+1}{\gamma-1}\right)\left(\frac{R}{8\pi MT}\right)^{1/2} p \tag{2.75}$$

In this expression, α is the combined accommodation coefficient, given by

$$\alpha = \frac{\alpha_1\alpha_2}{\alpha_1+\alpha_2-\alpha_1\alpha_2} \tag{2.76}$$

where

α_1, α_2	are	accommodation coefficients for the gas molecules at the two surfaces;
γ		specific heat ratio for the gas, nondimensional;
M		molar mass of the gas, in g/mol;
T		temperature intermediate between the temperatures of the surfaces, in K;
R		gas constant, R = 8.314 J/Kmol;
p		pressure, in Pa.

The predominant gas species in degraded samples of vacuum glazing has been determined to be water vapor. Water molecules interact strongly with the internal surfaces of the glazing. Assuming a combined accommodation coefficient of 0.9, the gaseous conductance in the low pressure region is approximately

$$\Lambda_g = 0.8p \tag{2.77}$$

In order to ensure that gaseous conduction is negligible, the pressure within the glazing should therefore be less than about 0.1 Pa [63].

2.6.4. Optical properties

Optical properties of cover glazing are described by transmittance τ_{gl}, reflectance ρ_{gl} and absorptance α_{gl}. Each term is generally angular dependent. Sum of these three parts at each angle gives unity. Optical properties of absorber are given by absorptance α_{abs} and reflectance ρ_{abs} both angular dependent.

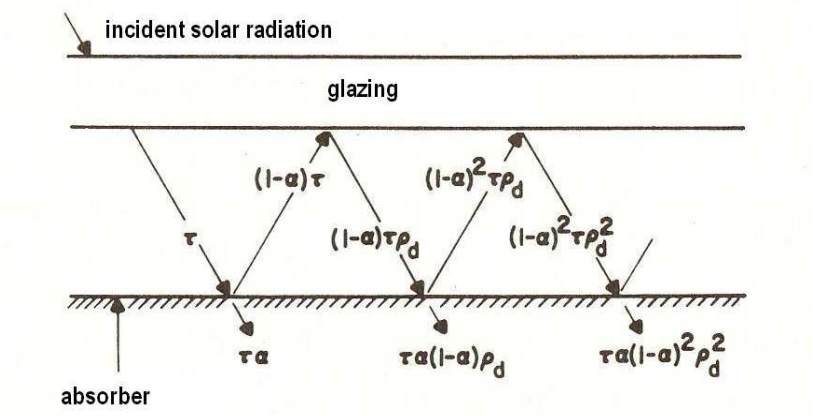

Fig. 2.18 – Absorption of solar radiation by absorber under cover glazing

An important factor if evaluating optical performance of solar collector is transmittance-absorptance product ($\tau\alpha$) as a complex property of cover-absorber combination. Product considers solar radiation passing through the cover to absorber and multiple reflections between absorber and cover glazing. The reflection from absorber plate is assumed to be diffuse, so the fraction (1 - α)τ that strikes cover is diffuse radiation and (1 - α)$\tau\rho_d$ is reflected back to absorber. As multiple reflection of diffuse radiation continues the fraction of the incident energy ultimately absorbed is

$$(\tau\alpha) = (\tau\alpha)\sum_{n=0}^{\infty}[(1-\alpha)\rho_d]^n = \frac{\tau\alpha}{1-(1-\alpha)\rho_d} \tag{2.78}$$

Diffuse reflectance ρ_d for diffuse radiation is usually estimated as reflectance for incidence angle 60° (single glazing usually 0.15, d ouble glazing 0.22).

3. Design tool KOLEKTOR

Mathematical model of solar thermal flat-plate liquid collector has been transformed into design tool KOLEKTOR 2.2. The design tool is a computer program with user-friendly interface created in Visual Basic Studio environment. Detailed geometrical and physical parameters of individual solar collector elements as well as operation & climatic boundary conditions are entered through appropriate tool cards (general design parameters, absorber, glazing, frame / insulation, calculation, see *Figs. 3.1 to 3.4*). Besides the principle parameters and characteristics the tool allows to enter also gas pressure inside the collector box (for modeling both flat-plate atmospheric and evacuated collectors), slope of collector, type of heat transfer fluid (water, water-ethyleneglycol solution, water-propyleneglycol solution with defined mixing ratio) and to choose the separate free-standing installation or building envelope integration of collector (with given thermal resistance of building envelope). Design tool allows to choose from various empirical models for calculating the heat transfer coefficients (e.g. forced convection in pipes, natural convection in gas layers, sky radiation, wind convection) collected from different authors and thus to trace the influence of heat transfer coefficient model selection on the calculated performance of solar collector.

3.1. Visual Basic

Visual Basic (VB) is the third-generation event-driven programming language and associated development environment (IDE) from Microsoft for its COM programming model. VB is also considered a relatively easy to learn and use programming language, because of its graphical development features and BASIC heritage.

Visual Basic was derived from BASIC and enables the rapid application development (RAD) of graphical user interface (GUI) applications, access to databases using Data Access Objects DAO, Remote Data Objects RDO, or ActiveX Data Objects ADO, and creation of ActiveX controls and objects. Scripting languages such as VBA and VBScript are syntactically similar to Visual Basic, but perform differently.

A programmer can put together an application using the components provided with Visual Basic itself. Programs written in Visual Basic can also use the Windows API, but doing so requires external function declarations.

The final release was version 6 in 1998. Microsoft's extended support ended in March 2008 and the designated successor was Visual Basic .NET.

3.2. .NET Framework

The Microsoft .NET Framework is a software technology that is available with several Microsoft Windows operating systems. It includes a large library of pre-coded solutions to common programming problems and a virtual machine that manages the execution of programs written specifically for the framework. The .NET Framework is a key Microsoft offering and is intended to be used by most new applications created for the Windows platform.

The pre-coded solutions that form the framework's Base Class Library cover a large range of programming needs in a number of areas, including user interface, data access, database connectivity, cryptography, web application development,

numeric algorithms, and network communications. The class library is used by programmers, who combine it with their own code to produce applications.

Programs written for the .NET Framework execute in a software environment that manages the program's runtime requirements. Also part of the .NET Framework, this runtime environment is known as the Common Language Runtime (CLR). The CLR provides the appearance of an application virtual machine so that programmers need not consider the capabilities of the specific CPU that will execute the program. The CLR also provides other important services such as security, memory management, and exception handling. The class library and the CLR together compose the .NET Framework.

The .NET Framework is included with Windows Server 2008 and Windows Vista. The current version of the framework can also be installed on Windows XP and the Windows Server 2003 family of operating systems. A reduced "Compact" version of the .NET Framework is also available on Windows Mobile platforms, including Smartphones.

3.3. Installation

Design tool KOLEKTOR 2.2 is developed in Visual Basic.NET platform. To start the tool, the distribution pack for Microsoft NET. Framework has to be installed first. If user has installed earlier pre-release versions of .NET Framework, then he must uninstall them prior to running this installation by using Add or Remove Programs. Last version of Microsoft NET Framework 3.5 can be downloaded from Microsoft website:

<http://www.microsoft.com/downloads/>

or with use of link from KOLEKTOR website:

<http://www.fsid.cvut.cz/~matuskat/kolektor/>

First step:	Download and install Microsoft.NET Framework 3.5
Second step:	Download *KOLEKTOR22.zip* pack from KOLEKTOR website to Program Files folder and unzip it. Folder Kolektor with installation files will be created.
Third step:	Start *setup.exe* and tool KOLEKTOR 2.2 will be installed into your computer and ready for first use. You can find it as an icon in Programs Menu under Kolektor or you can use *setup.exe* file (previously used for installation) for launching the program.

3.4. General functions

3.4.1. Roll window File

Open:	Opens file with input parameters of collector, operation, climate and models selection
Save:	Saves file with input parameters of collector, operation, climate and models selection. Data entered into tool cards and selections made can be saved into text file (*.kol) for later use.

3.4.2. Roll window Calculation

Start calculation: Runs the calculation process

Results export Results of calculation (collector efficiency curve) can be saved into spread-sheet file (*.res).

3.4.3. Roll window Help

Short information on design tool is added.

3.5. Cards

Individual cards are used to input parameters of collector, operation, climate and models selection.

3.5.1. General parameters

Card (see *Fig. 3.1*) contains operation and climatic conditions, including the slope of collector and parameters of adjacent structures (emittance of surfaces, resistance of envelope) and principle geometry of solar collector (gross and aperture size, depth of collector).

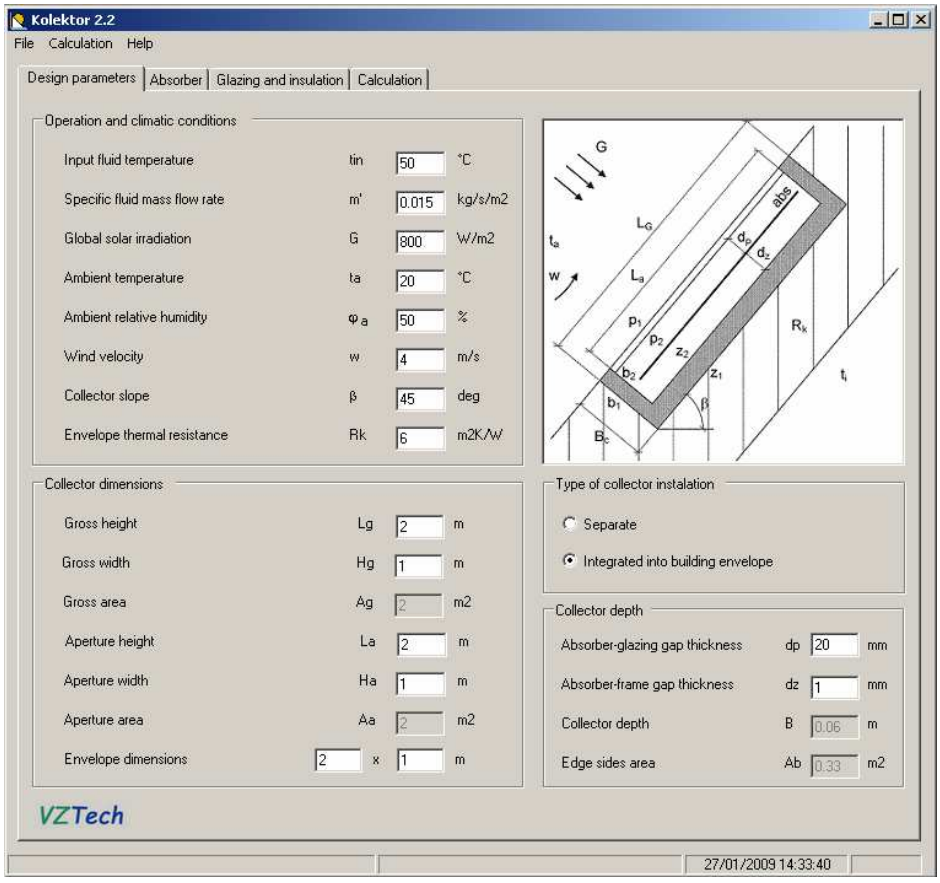

Fig. 3.1 – Design parameters card

Input temperature t_{in} is used only if calculation of single working point is chosen.

Card contains also either/or specification whether collector is installed separately from building envelope (emittance of adjacent envelope surface as input) or integrated into building envelope (thermal resistance of building envelope as input).

3.5.2. Absorber

Card contains specification of absorber plate properties (material, emittances) and pipe register geometry and thermal bond specification (see *Fig. 3.2*).

Absorber material selection has predefined following items with appropriate thermal conductivity values:

copper (default) 390 W/mK;

aluminium 250 W/mK;

steel 100 W/mK.

Type of bond absorber-riser pipe selection has predefined following items attended by appropriate figure (see chapter internal balance):

upper bond;

side bond;

lower bond.

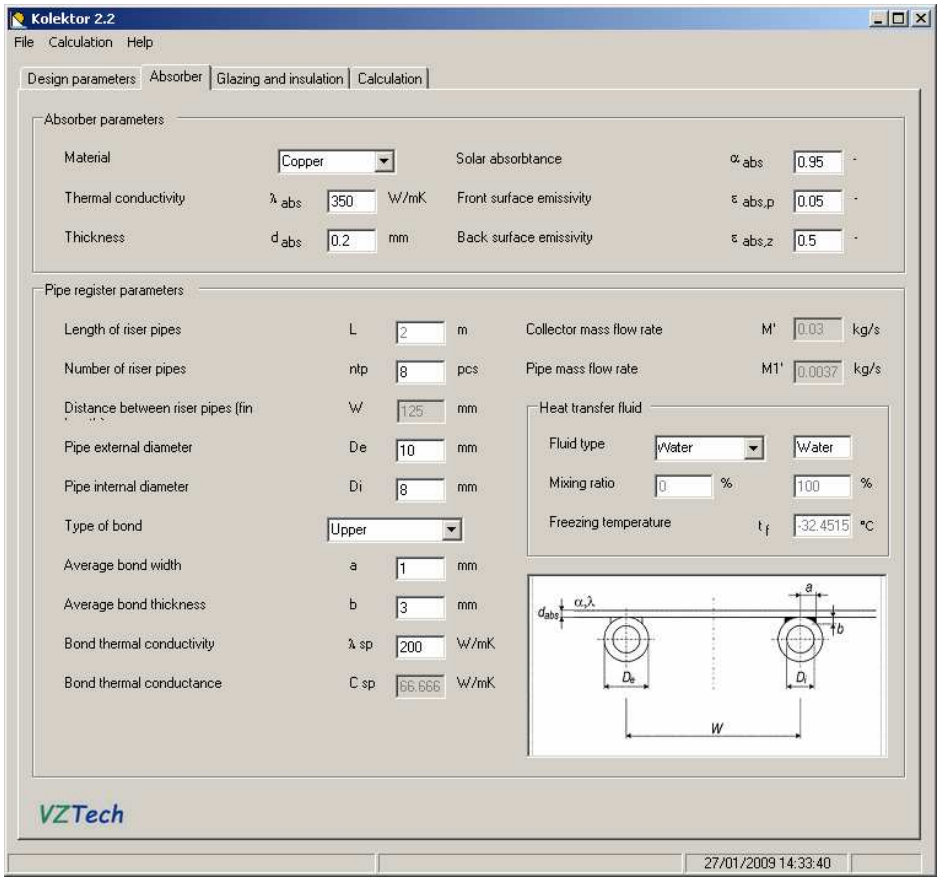

Fig. 3.2 – Absorber card

3.5.3. Glazing and insulation

Card contains thermal and optical properties of glazing and thermal properties of frame (insulation). Thermal properties of glazing can be entered by means of thermal conductivity dependent on mean temperature (suitable for glazing structures like

transparent insulations) or just as a single value for thermal resistance of glazing. Optical properties of glazing are specified for normal incidence. Optical efficiency of solar collector is calculated at right lower part of card.

As a special feature gas filling pressure inside the collector box can be used as input. At this moment just air can be considered as collector box filling.

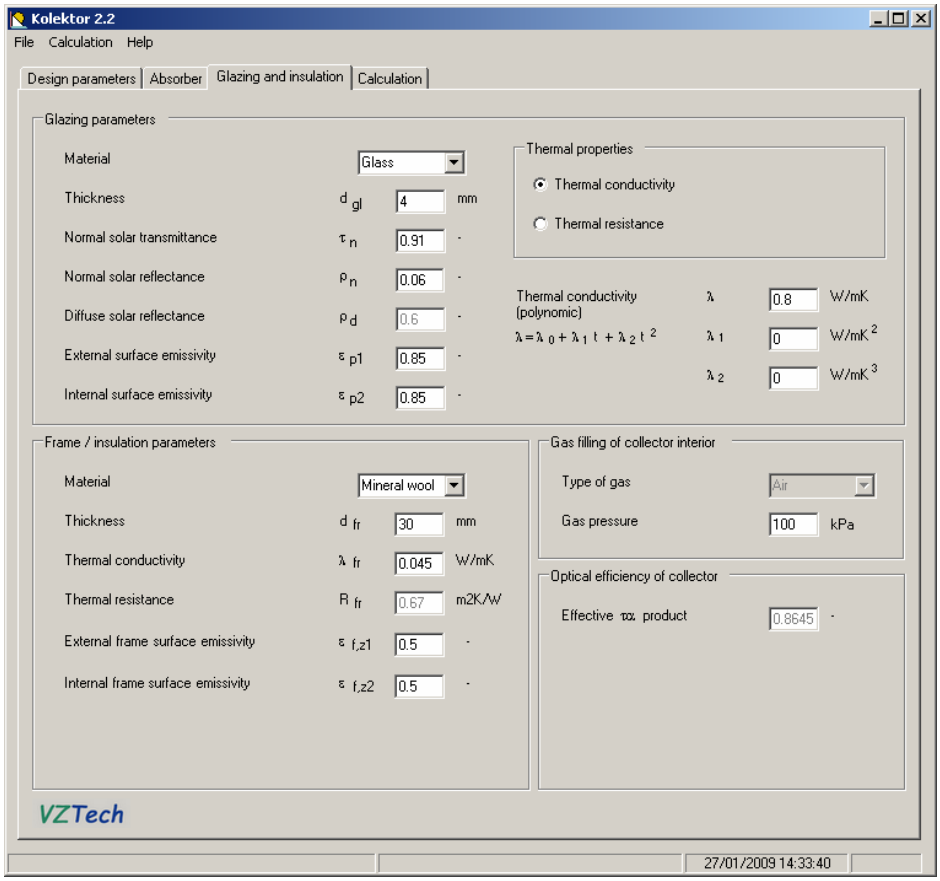

Fig. 3.3 – Glazing and frame / insulation card

Frame insulation material selection has predefined following items with appropriate thermal conductivity values:

polyurethane (default)	0.035 W/mK;
mineral wool	0.040 W/mK.

3.5.4. Calculation

Calculation card shows the layout of solar collector (glazing, absorber, frame insulation), surface temperatures, roll windows with individual selection of heat transfer models and corresponding values of heat transfer coefficients (displayed after calculation).

Selection of models is used here due to high number of possible models for calculation of heat transfer coefficients available but with rather different resulting values, e.g. wind convection models, and their influence on calculated collector performance should be verified (sensitivity analysis).

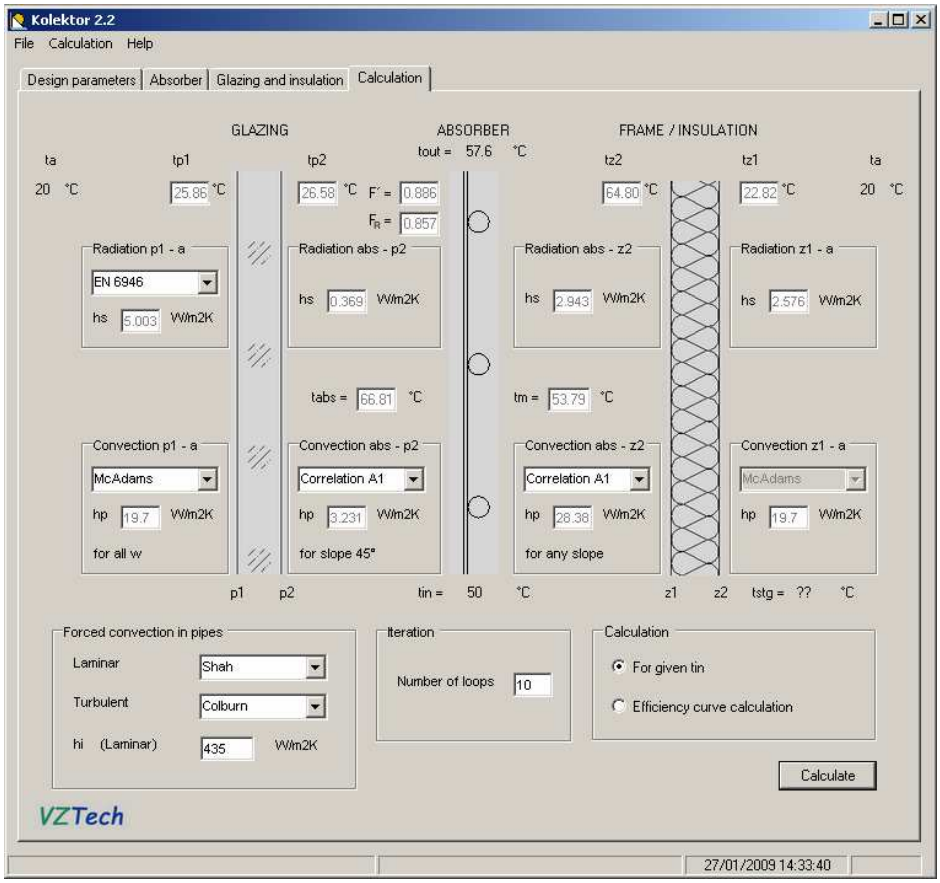

Fig. 3.4 – Calculation card

Calculation mode can be specified as single working point calculation or efficiency curve calculation. If single point calculation selected input temperature t_{in} and climatic condition are used as boundary conditions. Efficiency curve mode calculates the individual efficiency points for given climatic conditions (default values recommended) and input temperature t_{in} in the range from 20 to 400 ℃ and results are related to:

mean absorber temperature	$(t_{abs} - t_a)/G$
mean fluid temperature	$(t_m - t_a)/G$
input temperature	$(t_{in} - t_a)/G$

Number of iteration loops can be set (default value 10 is recommended).

Nominal stagnation temperature t_{stg} is displayed for extreme conditions (G = 1000 W/m^2, t_a = 30 ℃). Calculation of stagnation temperature is available only in the mode of efficiency curve calculation. If stagnation temperature is not found, value "???" appears instead of value.

3.6. Troubleshooting

3.6.1. Local decimal settings

Problems concerning to use of dot instead of comma has been solved. User of design tool should work in local setting of windows using dot in decimal values (e.g. Great Britain), all default and entered values should be input with dot (if in decimal form). Else the program cannot calculate and message “NaN” appears in the boxes.

4. Experimental evaluation of the model

Mathematical model KOLEKTOR 2.2 has been experimentally validated in the frame of solar collectors testing according to European standard [2] in the Solar Laboratory operated under Department of Environmental Engineering at Faculty of Mechanical Engineering, Czech Technical University in Prague [3]. Solar thermal collectors have been tested to obtain steady state performance thermal output at constant operation conditions of inlet temperature (± 0,1 K) and mass flow rate (± 1 %) of heat transfer fluid (water) entering collector and at constant climatic conditions of solar irradiation (± 50 W/m^2) and ambient temperature (± 0,5 K). Instantaneous efficiency has been calculated from collector thermal output related to total solar irradiation input (incident on collector reference area: aperture area). The efficiency curve (dependence of efficiency on mean reduced temperature difference) has been obtained from at least 6 points in the range of input fluid temperature from ambient (around 20 ℃) to 90 ℃. Experimental data points of solar collector efficiency are coupled with uniform uncertainty bars in the graphs. Expanded efficiency uncertainty has been assessed for experimental data from both type A (statistical) and type B (instrumental) uncertainties considering the coverage factor 2 with 95% level of confidence [66, 67] and for usual steady state conditions of measurements lies between 3 and 4 %.

Mathematical model has been validated in the field of atmospheric solar flat-plate collectors (nonselective absorber without conductive bond to register pipes; high-quality solar collector with state-of-art copper laser welded absorber coated with high performance selective coating and solar antireflective glazing) and in the field of evacuated solar flat-plate collectors. Experimental validation of evacuated type has been performed on commercial solar flat-plate vacuum collector with selective absorber and no insulation applied at the back of absorber (only air layers at given pressure). The collector envelope consisting of low iron glazing and moulded metal frame is equipped with pressure valve inlet for repeatable evacuation. Support pillars to bear the glazing at condition of underpressure stress are placed between the glazing and back side of the collector and penetrating the absorber through holes (elimination of thermal bridges, not considered in modeling). The atmospheric variant of the collector (interior pressure 100 kPa) has been evaluated as a reference case (atmospheric selective collector – but without insulation). The evacuated variant of the collector has been tested with interior pressure reduced and maintained by vacuum pump at 9 kPa. Experimental data and efficiency curves calculated from model have been graphically compared (see *Fig. 4.1* and *Fig. 4.2*).

The theoretical calculation of efficiency curve by model is subjected to uncertainty of input parameters. While geometrical parameters are easily available with high degree of confidence, number of parameters defining the properties of collector parts is found uncertain within narrow range (e.g. absorber and glazing properties parameters, mostly ± 1 %), middle range (e.g. conductivity of insulation layer dependent on its temperature and density, ± 10 %) and quite broad range (e.g. emittance of absorber back side, insulation or collector frame, > 50 %). Each of varying parameter has a different impact (sensitivity) to resulting efficiency value from high effect of absorber and glazing optical properties to negligible effect of frame external surface emittance. Uncertainty of input parameters and its influence to calculated efficiency has been expressed by two borderlines where the collector efficiency values can be found in reality.

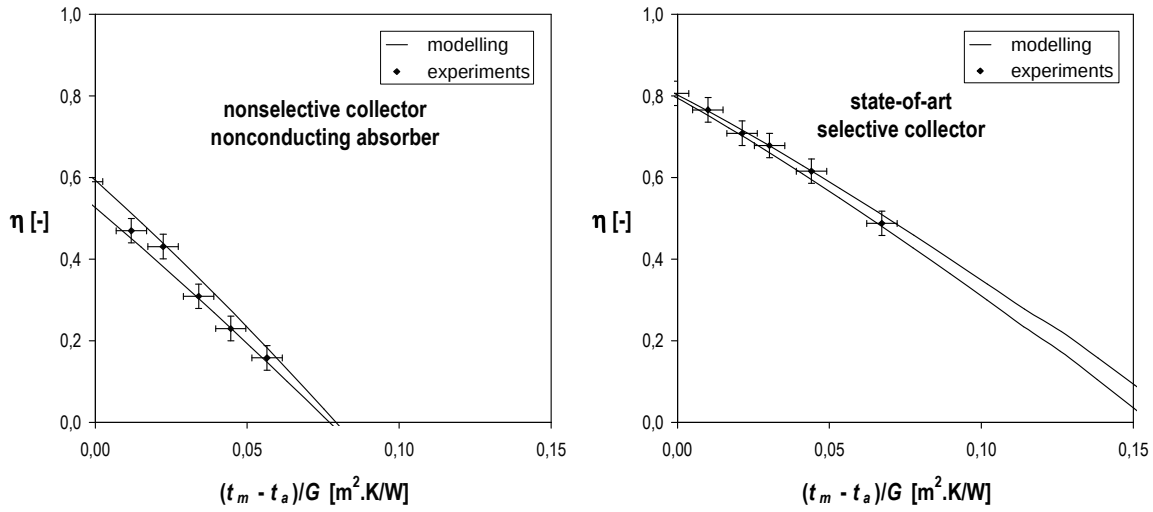

Fig. 4.1 – Experimental evaluation of the mathematical model by collector testing (different absorber quality)

Fig. 4.1 shows validation of the model for two examples of different atmospheric flat-plate collectors. Collector on the left consists of nonselective absorber without conductive bond to register pipes (steel absorber is bond to copper pipe only by spot grip-contact). Standard safety glazing and mineral wool insulation are used in its construction. Determination of absorber-pipes bond conductance is a main source of uncertainty in the calculation.

Collector on the right is a representative of high-quality solar collectors with state-of-art copper laser welded absorber. High performance selective coating and solar antireflective glazing properties from optical testing reports were provided thus reducing the uncertainty of calculation to very low values. Due to sufficient back side insulation the influence of uncertain internal and external surfaces emittance has decreased to minimum.

Mathematical model has been also tested in the field of solar flat-plate evacuated collectors. Validation has been performed on commercial evacuated collector with selective absorber and no insulation applied at the back of absorber (only air layers at given pressure). The collector envelope consists of moulded metal frame and low iron glazing. Support pillars to bear the underpressure stress are placed between glazing and back side of the collector and penetrating the absorber through holes (elimination of thermal bridges, not considered in modeling). The atmospheric variant of the collector (interior pressure 100 kPa) has been evaluated as a reference case (see *Fig. 4.2*, graph on the left). The evacuated variant has been tested with interior pressure reduced to 9 kPa (see *Fig. 4.2*, graph on the right).

All tested variants of solar collector construction have shown a good agreement between the modeled and experimentally obtained solar collector efficiency curves within the range caused by uncertainty of model input parameters (uncertain values of thermal properties of used materials, optical properties of surfaces, etc.).

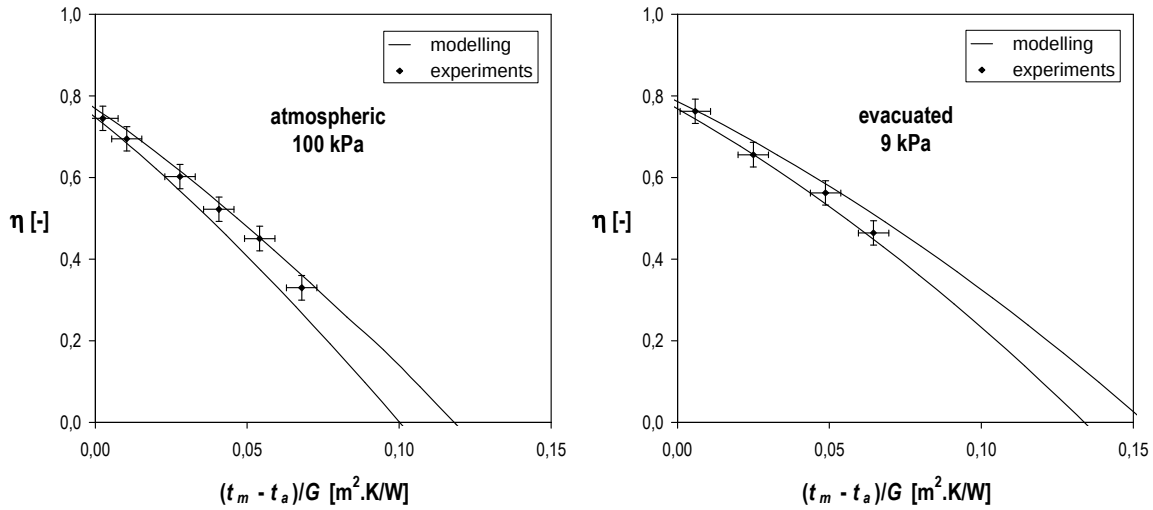

Fig. 4.2 – Experimental evaluation of the mathematical model by collector testing (different interior pressure)

5. Outlook for future development

The model and design tool is under continuous development. Validation of the model for unglazed solar thermal collector type is planned and huge experimental investigations are expected due to high uncertainty in modeling of wind convection heat transfer coefficients known from literature. Mathematical model of solar thermal flat-plate collector (glazed, unglazed) and design tool KOLEKTOR will stand as a basis for development of universal solar photovoltaic-thermal liquid collector model. Advanced PV/T model will allow PV collector modeling (fluid mass flow equal zero, considering influence of temperature on electric efficiency), PT collector modeling (PV reference efficiency equal zero) or PV/T collector modeling.

5.1. Next version

KOLEKTOR 3.1 will include:

- calculation of U_b separately from U_z – a number of solar collectors is equipped by different insulation layer for back side and edge side (different thickness)
- linear dependence of collector frame insulation thermal conductivity on mean temperature in the insulation layer
- rearrangement of cards – card glazing will be separate, and model will allow the possibility for theoretical calculation of optical properties of glazing from refraction index *n* and attenuation coefficient *K*

5.2. Far future outlook

Target of development of the software is:

- Multiple glazed collector (unglazed, single, double glazed collectors), including heat transfer through individual gas layers – it will need a complete rearrangement of calculation procedure.
- PV/T collector (unglazed, glazed) – absorber with electricity production (now finished in excel sheet for unglazed configuration, experimental validation in summer 2009).

6. Acknowledgement

The development of mathematical model and design tool KOLEKTOR has been supported by research project MSM 684077011 “Environmental Engineering” granted by Ministry of Education, Youth and Sports.

The experimental validation of the model has been supported by research project CTU 88059012 „Experimental validation of mathematical model for flat-plate evacuated solar thermal collector“.

7. Nomeclature

Nomenclature generally results from usual symbols used in solar thermal engineering.

7.1. Latin symbols

a	thermal diffusivity	m^2/s
a	bond width	m
A_a	collector aperture area	m^2
A_G	collector gross area	m^2
b	bond thickness	m
C_{sp}	bond thermal conductance	W/mK
c	specific thermal capacity	J/kgK
D_e	external pipe diameter	m
D_i	internal pipe diameter	m
F	fin efficiency	-
F'	collector efficiency factor	-
F_R	collector heat removal factor	-
g	gravity acceleration	m/s^2
G	solar irradiation	W/m^2
h_i	convection heat transfer coefficient inside riser pipe	W/m^2K
h_w	wind convection heat transfer coefficient	W/m^2K
L	length, thickness	m
$\dot{M}$	mass flow rate	kg/s
p_d	water vapor pressure	Pa
$p"_d$	saturated water vapor pressure	Pa
q	heat flow density	W/m^2
$\dot{Q}_s$	solar irradiation incident on collector area	W
$\dot{Q}_{l,o}$	optical loss	W
$\dot{Q}_{l,t}$	heat loss	W
$\dot{Q}_u$	useful thermal power from collector	W
t	Celsius temperature	℃
t_{abs}	absorber temperature	℃
t_a	ambient temperature	℃
t_{dp}	dew point temperature	℃

T	absolute (Kelvin) temperature	K
U_p	heat loss coefficient for front side of the collector	W/m^{2}K
U_z	heat loss coefficient for back side of the collector	W/m^{2}K
U_b	heat loss coefficient for edge side of the collector	W/m^{2}K
W	fin width, distance between risers	m

7.2. Greek symbols

α	solar radiation absorptance of collector absorber	-
β	volumetric thermal expansion coefficient	1/K
δ	thickness of absorber	m
ε	emittance	-
ε_o	sky emittance	-
η	efficiency	-
ϕ	slope angle	deg
λ	thermal conductivity	W/mK
ν	kinematic viscosity	m^2/s
ρ	density	kg/m^3
σ	Stefan-Boltzman constant	
τ	solar radiation transmittance of collector cover glazing	-

7.3. Criterial numbers

Gr	Grashof number
Gz	Graetz number
Nu	Nusselt number
Pr	Prandtl number
Ra	Rayleigh number
Re	Reynolds number

7.4. Indices

7.4.1. Main surfaces

Indices for description of main collector surfaces were introduced from Czech version to avoid nomenclature collisions:

p	front side (from Czech “přední”)
z	back side (from Czech “zadní”)
b	edge side (from Czech “boční”)
1	exterior surface

2 interior surface

Relationship between two surfaces e.g. identifying distance is expressed by combination of the indices. The order of indices is given by supposed heat flow direction (from absorber to ambient).

Example 1: $L_{abs\text{-}p2}$ is thickness of gas layer between absorber and surface p2 (interior surface of front cover glazing).

Example 2: $T_{abs\text{-}z2}$ is mean temperature in gas layer between absorber and surface z2 (interior surface of back side frame).

7.4.2. Heat transfer modes

Indices for description of heat transfer modes were introduced from Czech version for better one-letter distinction:

p convection heat transfer (from Czech "proudění")

v conduction heat transfer (from Czech "vedení")

s radiation heat transfer (from Czech "sálání")

7.4.3. More indices

a aperture

a ambient

f fluid

fr frame

g gas layer

G gross

in input

out output

sp bond

8. References

[1] Duffie, J. A., Beckman, W. A.: Solar Engineering of Thermal Processes. 3rd edition, Wiley & Sons, Inc., 2006.

[2] Goswami, D. Y., Kreith, F., Kreider, J. F.: Principles of Solar Engineering, 2nd edition, Taylor & Francis, 1999.

[3] Solar Energy – The State of Art, ed. by J. Gordon (ISES), James & James, 2001.

[4] TRNSYS 16 release, Mathematical reference, Wisconsin University, 2004.

[5] Fraisse, G., Plantier, Ch.: Development and experimental validation of a detailed flat-plate solar collector model, 5th European TRNSYS user meeting, 2003.

[6] Koo, J.: Development of a Flat-Plate Solar Collector Design Program, Master Thesis. University of Wisconsin-Madison, 1999.

[7] Hottel, H. C., Woertz, B. B.: The performance of flat plate solar heat collectors. Transactions of ASME, No. 64, pp. 91-104, 1942.

[8] Klein, S. A.: Calculation of Flat-Plate Collector Loss Coefficient. Solar Energy Vol. 17, pp. 79, 1975.

[9] Agarwal V. K. and Larson D. C. (1981) Calculation of top loss coefficient of a flat plate collector. Solar Energy 27, 69–71.

[10] Malhotra A., Garg H. P. and Palit A. (1981) Heat loss calculation of flat-plate solar collectors. Journal of Thermal Engineering (Journal of the Indian Society of Mechanical Engineers) 2(2), 59–62.

[11] Garg, H. P., Datta, G.: The top loss calculation for flat plate solar collectors, Solar Energy, Volume 32, Issue 1, Pages 141-143, 1984.

[12] Matuska, T.: Transparent thermal insulations and their use in solar energy applications, Ph.D. thesis, CTU in Prague, 2003.

[13] ISO 6946. Building components and building elements - Thermal resistance and thermal transmittance - calculation method 1996.

[14] Swinbank, W., C.: Long-wave radiation from clear skies. Quarterly Journal of Royal Meteorological Society 89, pp. 339-348, 1963.

[15] Bliss, R., A.: Atmospheric radiation near the surface of the ground: a summary for engineers. Solar Energy 5, pp. 103-120, 1961.

[16] Berdahl, P., Martin, M.: Emittance of clear skies, Solar Energy 32 (5), pp. 663-664, 1984.

[17] Brunt, D.: Notes on radiation in the atmosphere, Quarterly Journal of the Royal Meteorological Society. 58, pp. 389-418, 1932.

[18] Aubinet, M.: Longwave sky radiation parametrizations. Solar Energy 53 (2), pp. 147-154, 1994.

[19] Berger, X., Buriot, D., Garnier F.: About the equivalent radiative temperature for clear skies. Solar Energy 32 (6), pp. 725-733, 1984.

[20] Incropera, F. P., DeWitt, D. P.: Fundamentals of heat and mass transfer, 4th edition, Wiley, New York, 1996.

[21] McAdams, W. H.: Heat Transmission, 3rd edition. McGraw-Hill, New York. pp. 249. 1954.

[22] Jürges, W.: Der Wärmeübergang an einer ebenen Wand, Behifte zum Gesundheits-Ingenieur, Reihe 1, Beiheft 19, München, 1924.

[23] Watmuff J.H., Charters, W.W.W, Proctor, D.: Solar and wind induced external coefficients for solar collectors, Int. Revue d'Hellio-technique Vol. 2, pp. 56, 1977.

[24] Sparrow, E. M., Tien, K. K.: Forced convection heat transfer at an inclined and yawed square plate, application to solar collectors. ASME J. Heat Transfer 99, 507-512 (1977).

[25] Tien, Sparrow: Local heat transfer and fluid flow characteristics for airflow oblique or normal to a square plate. Int J. Heat Mass Transfer, Vol. 22, pp. 349-360, 1979

[26] Sparrow, E. M. et al.: Effect of finite width on heat transfer and fluid flow about an inclined rectangular plate. Trans. ASME J. Heat Transfer 101, pp. 2, 1979.

[27] Sparrow, E. M., Lau, S. C.: Effect of adiabatic co-planar extension surfaces on wind-related solar-collector heat transfer coefficient. Transactions of ASME – Journal of Heat Transfer 103, 268-271, 1981.

[28] Kowalski, G. J., Mitchell, J. W.: Heat transfer from spheres in the naturally turbulent outdoor environment. ASME J. Heat Transfer 89, 649-653, 1976.

[29] Test, F. L., Lessmann, R. C.: An experimental study of heat transfer during forced convection over a rectangular body. Transactions of ASME – Journal of Heat Transfer, Vol. 102, 146-151, 1980.

[30] Test, F. L, Lessmann, R. C., Johary, A.: Heat transfer during wind flow over rectangular bodies in the natural environment. ASME J. Heat Transfer 103, 262-267, 1981.

[31] Kind, R. J., Gladstone, D. H., Moizer, A. D.: Convective heat losses from flat-plate collectors in turbulent winds. Transactions of ASME, J. Solar Energy Engg 105, 80-85, 1983.

[32] Kind, R., J., Kitaljevich, D.: Wind-induced heat losses from solar collector arrays on flat-roofed buildings. Transactions of ASME, J. Solar Energy Engg 107, 335-342, 1985.

[33] Kumar, S., Sharma, V. B., Kandpal, T. C., Mullick, S. C.: Wind induced heat losses from outer cover of solar collector. Renewable Energy, Vol. 10, No. 4, pp. 613-616, 1997.

[34] Sharples, S., Charlesworth, P. S.: Full-scale measurements of wind-induced convective heat transfer from a roof-mounted FPC. Solar Energy, Vol. 62, No. 2, pp. 69-77, 1998.

[35] Johnson R. R., Othieno, H.: Estimated wind related heat transfer coefficients for flat plate solar collectors.

[36] Hollands et al.: Free convective heat transfer across inclined air layers, Transactions of ASME, Journal of Heat Transfer Vol. 98, pp. 189-193, 1976

[37] Buchberg, Catton, Edwards: Natural convection in enclosed spaces - a review of application to solar energy collection, Transactions of ASME, Journal of Heat Transfer Vol. 98, pp. 182-188, 1976

[38] Randall, Mitchell, El-Wakil: Natural convection heat transfer characteristics of flat-plate enclosures, Transactions of ASME, Journal of Heat Transfer Vol. 101, pp. 120-125, 1979

[39] Schinkel, W. M. M.: Natural convection in inclined air-filled enclosures, ISBN 90-6231-079-6. ed. Dutch Efficiency Bureau 1980.

[40] Yin, Wung, Chen: Natural convection in an air layer enclosed within rectangular cavities, Int. j. Heat Mass Transfer, Vol. 21, pp. 307-315, 1977

[41] Sazima, M., Kmoníček, V., Schneller, J. a kol.: Technický průvodce - Teplo. SNTL Praha 1989. ISBN 80-03-00043-2.

[42] Arnold, Catton, Edwards: Experimental investigation of natural convection in inclined rectangular regions of differing aspect ratios. ASME Paper 75-HT-62, 1975.

[43] Recknagel, H., Sprenger, E., Schramek, E.R.: Taschebuch für Heizung und Klimatechnik 1994/1995. Oldenburg. ISBN -3486-26213-0.

[44] reserve

[45] reserve

[46] Hausen, H.: Neue Gleichungen für die Wärmeübertragung bei freier oder erzwungener Strömung, Allg. Waermetech, Vol.9, pp. 75-79, 1959

[47] Bejan, A.: Convective heat transfer, 2nd edition, John Wiley and Sons, Inc. 1995.

[48] Jacob, M.: Heat transfer, Vols. I and II, John Wiley and Sons, Inc., New York, 1949, 1957.

[49] Sleicher, C. A., Rouse, M. W.: Int. J. Heat Mass Transfer, vol. 18, pp. 677-683, 1975.

[50] Shah, R. K., London, A. L.: Laminar flow forced convection in ducts. 1st edition. New York: Academic Press. 1978.

[51] Kays, W.M., Crawford, M.E.: Convective heat and mass transfer, 3rd edition. McGraw-Hill, Inc. 1993. ISBN 0-07-112516-7.

[52] Hausen, H.: Z. Ver. Dtsch. Ing. Beih. Verfahrenstech., Vol. 91, No. 4.

[53] Sieder, E. N., Tate, G. E.: Heat transfer and pressure drop of liquids in tubes. Ind. Eng. Chem., Vol. 28, pp. 1429-1436, 1936.

[54] Churchill, Ozoe, lost reference

[55] Colburn, A. P.: Trans. AIChE, 29, 174, 1933.

[56] Dittus, P. W., Boelter, L. M. K.: Heat transfer in automobile radiators of the tubular type. University of California Publications on Engineering, Vol. 2, No. 13, p. 443-461, Berkeley, 1930; reprinted in Int. Commun. Heat Mass Transfer, vol. 12, pp. 3-22, 1985.

[57] Petukhov, B. S., in T. F. Irvine and J. P. Hartnett, Eds. Advances in Heat Transfer, Vol. 6, Academic Press, New York, 1970.

[58] Gnielinski, V.: New equations for heat and mass transfer in turbulent pipe and channel flow, Int. Chem. Engineering. Vol. 16, pp. 359-368, 1976.

[59] Kakac, S., Shah, R. K., Aung, W.: Handbook of single-phase convective heat transfer, Wiley, New York, 1987.

[60] Conde, M.: Thermophysical properties of brines – Models, Conde Engineering, http://www.mrc-eng.com, Zurich 2002.

[61] Potkay, J. A., Lambertus, G. R., Sacks, R. D., and Wise, K. D.: A low pressure- and temperature- programmable mGC column," Solid-State Sensor, Actuator and Microsystems Workshop, Hilton Head Island, SC, USA, June 2006, pp. TBD.

[62] Corrucini, R. J.: Gaseous heat conduction at low pressures and temperatures. Vacuum 7–8, pp. 19–29, 1957.

[63] Collins, R. E., Simko, T. M.: Current status of science and technology of vacuum glazing, Solar Energy Vol. 62, No. 3, pp. 189–213, 1998.

[64] Sparrow, E. M., Tien, K. K.: Forced convection at an inclined and yawed square plate – application to solar collectors. ASME Journal of Heat Transfer, Vol. 99, pp. 507-512, 1977.

[65] Sparrow, E. M., Lau, S. C.: Effect of adiabatic co-planar extension surfaces on wind-related solar collector heat transfer coefficients. ASME Journal of Heat Transfer, Vol. 103, pp. 268-271, 1981.

[66] Mathioulakis, E., Vorostopoulos, K., Belessiotis, V.: Assessment of Uncertainty in Solar Collector Modeling and Testing. Solar Energy 66, 337-347, 1999.

[67] Müller-Schöll, Ch., Frei, U.: Uncertainty Analyses in Solar Collector Measurement. Proc. of Eurosun 2000, Copenhagen, 2000.

[68] T. Matuska, V. Zmrhal, Software tool KOLEKTOR 2.2, available from <http://www.fsid.cvut.cz/~matuskat/kolektor>